Actin Depolymerization Factors (ADFs) Moonlighting: Nuclear Immune Regulation by Interacting with WRKY Transcription Factors and Shaping the Transcriptome

Pai Li[1,2,3*], Brittni Kelley[4], Zizhang Li[3], Bruce Procter[1,5], Alex Corrion[1,2,9], Xuan Xie [6], Ryan Sheick[7], Yi-ju Lu[1,8], Mika Nomoto[9], Cheng-i Wei[10], Yasuomi Tada[9], Sheng-yang He[7,11,12], Shunyuan Xiao[3,13,*], Brad Day[1,14,*]

[1]Department of Plant, Soil and Microbial Sciences, Michigan State University, East Lansing, MI 48824, USA
[2]Department of Plant Biology, Michigan State University, East Lansing, MI 48824, USA
[3]Institute for Bioscience and Biotechnology Research, University of Maryland, Rockville, MD 20850, USA
[4]Plant Resilience Institute, Michigan State University, MI 48824, USA
[5]Lyman Briggs College, Michigan State University, MI 48824, USA
[6]Cell & Molecular Biology Program, Institute for Quantitative Health Science and Engineering, Michigan State University, East Lansing, MI 48824, USA
[7]MSU-DOE Plant Research Laboratory, Michigan State University, East Lansing, MI 48824, USA
[8]The Department of Plant Pathology and Microbiology, National Taiwan University, Taipei, 10617, Taiwan
[9]Center for Gene Research, Nagoya University, Furo-cho, Chikusa-ku, Nagoya, Aichi 464-8602, Japan
[10]Department of Nutrition and Food Science, University of Maryland College Park, MD 20742
[11]Howard Hughes Medical Institute, Duke University, Durham, NC 27708, USA
[12]Department of Biology, Duke University, Durham, NC 27708, USA
[13]Department of Plant Sciences and Landscape Architecture, University of Maryland College Park, MD 20742, USA
[14]Research and Innovation, University of Tennessee–Knoxville, Knoxville, TN 37996, USA

[*]Author for correspondence: Pai Li (lipai@umd.edu), Shunyuan Xiao (xiao@umd.edu), Brad Day (bradday@utk.edu)

Abstract

Remodeling of the actin cytoskeleton during the activation of plant immunity is a critical process for the transport and stabilization of immune-regulatory organelles and molecules. In this process, actin depolymerization factors (ADFs) function as key player through both severing and depolymerizing actin microfilaments. However, recent evidence suggests that ADFs may possess non-canonical immune functions inside the nucleus, in addition to a cytosolic role, a phenomenon not adequately explained by the traditional mechanistic model of ADFs and actin. In this study, we demonstrate that ADFs indeed have a moonlighting function in the nucleus, interacting with transcriptional machinery and regulating the transcriptome during both resting states and immune responses. Specifically, ADF2/3/4 exhibit redundant functions in defense against virulent and avirulent Pseudomonas, but not certain species of Pectobacterium and powdery mildew. Notably, nuclear – rather than cytosolic – ADFs contribute to defense against Pseudomonas and mediate pro-immune transcription. Mechanistically, we demonstrate that nuclear ADFs interact with transcription factors, histone complexes, and other components of the transcriptional machinery. Specifically, ADF2/3/4 can form a complex with WRKY transcription factors (such as WRKY22/29/48), thereby binding to promoters and directly regulating WRKY activity to shape the pro-immune transcriptome. In summary, our study reveals that ADFs moonlight as direct nuclear regulators of transcription factors, mediating a broad range of nuclear-cytoplasmic regulation of plant immunity and other processes.

Introduction

Plants have evolved complex immune systems, responsible for surveilling the environment to recognize and respond to potential threats, and in the case of biotic defenses, regulating specific, corresponding patterns of defense. Over the past three decades, the field of plant immunity has witnessed massive progress in the identification and characterization of core immune signaling mechanisms: from pathogen perception, signal cascading, pro-immune transcriptional reprogramming, as well as biochemical and morphological defensive responses (Jones et al. 2024). However, plant immunity is not a reductionist single-thread process. For example, even individual pathogens can generally introduce multiple PAMPs/DAMPs and avirulent effectors, mingling PTI and ETI into a dynamic and intertwined network across temporal and spatial scales (Yuan et al. 2021). Interestingly, while understanding the immune process as a complex "network" becomes an accurate and realistic perspective, it pushes a reductionist question to the foreground – *What central processes are dominating the entire immune network?*

Recently, a core participant of the conceptual immune signaling network has emerged in the shape of physical molecular network – the cytoskeleton – which presents a systemic and integral perspective towards a fuller understanding of plant immunity (Li and Day 2019; Wang et al. 2022; Lu et al. 2023; Sinha et al. 2024). To date, five types of cytoskeleton have been identified in eukaryotes: actin, microtubule, intermediate filament (Pollard and Goldman 2018), septin (Van Ngo and Mostowy 2019), and spectrin (Teliska and Rasband 2021), among which plants have two major types: actin and microtubules. Both are constructed by polymerized monomers that form filament meshwork that provides mechanical support to maintain cell shape and enable cellular and intracellular mobility. As one of the most important features of cytoskeleton, the architecture of cytoskeleton is highly dynamic, as both polymerization and depolymerization repetitively occur simultaneously towards an equilibrium. Therefore, this feature enables plants to actively re-model the cytoskeletal architecture to mediate desired cellular and physiological responses upon various signals, including immune activation. For example, inoculation of plants with virulent *Pseudomonas syringae* pv. tomato DC3000 (abbr. DC3000) has been shown to lead to increases in the density and bundling of actin filament of Arabidopsis epidermis cell in a global pattern (Li et al. 2022). In the case of filamentous pathogen, actin remodeling is usually observed as a condensed plate adjacent to haustorium or attempt penetration site (Qin et al. 2021; Sharma and Chandran 2022). Correspondingly, cytoskeletal remodeling is regarded as essential for both immunity and pathogenesis, as interfering cytoskeletal dynamics by cytoskeleton-targeted chemicals and effectors commonly leads to alternated resistance phenotype, but the direction of regulation varies in different cases (Li and Day 2019). At the mechanism level, these phenotypes are generally explained by the essential role of cytoskeleton in plasma membrane complex scaffolding and stabilization, as well as the directed transportation of pro-immune molecules and organelles (Li and Day 2019; Wang et al. 2022; Lu et al. 2023; Sinha et al. 2024).

Polymerization and depolymerization of actin filaments is facilitated by profilins and ADFs/cofilins, respectively (Lappalainen et al. 2022), and disabling the activity of either results in dampened immune signaling (Li and Day 2019). In the case of ADFs, multiple pieces of genetic evidence have demonstrated that specific ADFs in plants (e.g., Arabidopsis, barley, cotton, cucumber, common bean, and wheat) can regulate resistance to various types of pathogen, pests, and commensals (Sun et al. 2023). In most of these studies, while direct and detailed molecular mechanisms are lacking, it is generally accepted that the altered resistance phenotypes are attributed to the abnormal actin dynamics due to lack of ADF-driven actin depolymerization, a key step in actin remodeling in response to multiple immune signals (Li and Day 2019; Sun et al. 2023). However, a recent study from Inada et al. provides a distinctive insight into the relationship between ADF and immune signaling, which revealed that Arabidopsis subclass I ADFs (ADF1/2/3/4) contribute to the susceptibility to powdery mildew exclusively when these ADFs enter the nucleus (Inada et al. 2016). Because previous knowledge generally assumes, as noted above, that actin and its associated proteins (such as ADFs) facilitate immune process in the form of "canonic cytoskeleton" in the cytosol, the study by Inada and colleagues introduced an intriguing question related to the role of actin in plant immunity, or even general cell biology. *Does ADF – associated with actin – perform a moonlighting molecular function within the nucleus?*

In plants, the nuclear functions of ADF and actin are largely unknown. Conversely, studies in mammalian systems have shed light on potential mechanism(s) that engage actin and its dynamics in the nucleus. While predominantly localized in the cytosol, both mammalian actin and ADF have been shown to possess nuclear-localized roles. To enable this, cofilin, a member of ADF family, shuttles actin monomers (ACT) into the nucleus as cofilin-ACT complex, via a nuclear localization signal (NLS) recognized by importin-9 (Dopie et al. 2012). Inside nucleus, actin also exhibits morphological dynamic processes, partially resembling cytosolic actin cytoskeleton but with unique features. For example, nuclear actin remodel into nod-like structures upon chemical/environmental stress such hypoxia, pathogens, and drugs (Kloc et al. 2021), which is mechanistically associated with actin's interaction with RNA polymerases and chromatin remodeling complexes, a demonstrated role in transcriptional regulation (Kyheröinen and Vartiainen 2020; Wei et al. 2020). Interestingly, while no evidence yet suggests that canonic ADF can directly interact with transcriptional machinery without actin as the scaffold, it is reported that human Drebrin – and actin binding protein – utilizes its N-terminal ADF-H domain to interact with chromatin reader ZMYND8 to regulate its function (Yao et al. 2017). Finally, and with regard to the relationship between actin and immunity, it is noteworthy that ADF phosphorylation may be involved in the putative nuclear function. The mammalian cofilin is tightly regulated by phosphorylation (Xing et al. 2024), similar to ADFs of plants (Lu et al. 2020), whose phosphorylation, denoting a pro-immune phase, generally inhibits ADF-ACT interaction. In this manner, phosphorylation can potentially release ADF from actin to promote a different type of molecular function in the nucleus. In total, the evidence above supports the hypothesis that ADF possesses an

unknown transcriptional regulatory activity which is involved in, and contributes to, plant immunity.

In this study, we determined the genetic significance of nuclear ADFs in plant immunity and identified the historically described "ADF moonlighting function" as a transcription factor (TF) regulator in plant immunity. In brief, Arabidopsis ADF2/3/4 contribute to defense and directly interact with WRKY TFs and potentially other transcriptional machinery in the nucleus. In the specific case of ADF4 and WRKY29, they form an ADF-WRKY-DNA complex on the promoters of defense genes, which stabilizes the WRKY and further enhances its activity. As a result, nuclear – but not cytosolic – ADF4 majorly contributes to defense against *Pseudomonas syringae* by facilitating transcription of defense genes genome-widely, including pro-immune transcription factors such as WRKYs. However, the significance of cytosolic and nuclear ADFs in interaction with different pathogens and commensal microbes is not universal. Hence, we propose that the ADF possesses a moonlighting nuclear function as a direct transcriptional regulator, and that both cytosolic (for actin dynamics) and nuclear ADF (for transcription) are synergistically required for plant immunity and potentially other biological processes.

Results

Class I ADFs are expressed in leaves and redundantly contribute to defense.

Our previous study reported that an *adf4* mutant displays enhanced susceptibility against DC3000 harboring the avirulent effector protein AvrPphB, but not virulent, wild-type DC3000 (Tian et al. 2009; Porter et al. 2012). Since Arabidopsis has 11 *ADF* encoding genes, the products of which are small single-domain proteins without family-wide structural differences, we hypothesized that certain levels of functional redundancy may conceal potential immune functions of any given ADF. To begin to address the potential role *ADF* redundancy might play in the activation and signaling of plant immunity, we analyzed the expression profile of all *ADFs* during PTI and ETI signaling using published mRNA-seq datasets (GSE85932, (Birkenbihl et al. 2017); GSE151885, (Saile et al. 2020)). As shown in Fig. 1A, only ADF1/2/3/4 (class I), ADF5 (class III), and ADF6 (class IV) were found to be constitutively expressed in rosette leaves, with minor induction following immune elicitation in some of the cases. Considering the close phylogenic relationship among ADF1/2/3/4 (Fig. 1B) and the results of previous studies suggesting immune phenotypes in ADF1/2/3/4-silenced lines (Porter et al. 2012; Inada et al. 2016), we suspect that a high-order null mutant of class I ADFs will effectively abolish the activity of ADF.

Because *ADF1/2* and *ADF3/4* are adjacent genes (Fig. 1C), constructing high order mutants by crossing is impossible. Therefore, we used the CRISRP-Cas9 system to introduce null mutations of *ADF2* and *ADF4* to *adf1* and *adf3,* combined with crossing, to successfully obtain an *adf1/adf3/adf4* mutant (*a134*), and an *adf2/adf3/adf4* (*a234*) mutant (Fig. 1d, supp). However, the quadruple mutant *adf1/adf2/adf3/adf4* was not identifiable through repetitive efforts, potentially because losing all class I ADFs is lethal or results in infertility. We also obtained *adf6* through CRISPR-knockout; similarly, *adf2/adf3/adf4/adf6* was not identifiable.

Next, to determine the genetic contribution of leaf-expressed ADFs to immunity, we challenged the high-order mutants with DC3000 and DC3000/AvrPphB to evaluate the bacterial growth (see Fig. 1E-H). For DC3000, we observed a trend that more ADFs null mutations corelates with higher susceptibility, as *a134* and *a234* have ~10-fold higher susceptibility compared to Col-0 while *adf4-2b* has only 2~3 folds. When ETI was introduced by AvrPphB, such trend was maintained, and the contrast between Col-0 and *a234* is further increased. Indeed, Class I ADFs significantly and redundantly contribute to basal defense and potentially ETI against AvrPphB.

Nucleus ADF4 interacts with nuclear proteins including transcription machinery

As mentioned above, previous studies implied that nuclear ADF4 may play an independent role in immunity beyond its canonic function as an actin depolymerization catalyst within the cytosol (Inada et al. 2016). To explain those phenotypes, we hypothesize that ADFs can regulate the function of transcription machinery through an unknown mechanism. To determine the potential roles of ADF in the nucleus, we conducted a TurboID proteomic screening to identify nuclear interactors of ADF4 (Fig. 2). TurboID is engineered biotin ligase that generates unstable ATP-biotin intermediate at the presence of biotin, which immediately transfer the biotin to adjacent protein as a tag of interactors (Mair et al. 2019). Specifically, we adapted a engineered variant of TurboID with smaller size, namely miniTurbo (Branon et al. 2018), to create an ADF4-miniTurbo-mVenus-NLS (abbr. A4mTBYN; NLS, SV40 nuclear localization signal peptide) fusion protein construct, which was transformed into *a234* background to pull-down ADF4 interactor. A fusion without

ADF4 (abbr. mTBYN) was used as negative control (Fig. 2B, C). Confocal microscopy confirms that both constructs specifically localized in the nucleus, suggesting NLS is sufficiently active (Fig. 2D).

In order to identify ADF4 nuclear interactors associated with immunity, we challenged the 4-5-week-old Arabidopsis rosette leaves with a mixture of flg22 and elf18 (PAMPs that elicit PTI) 3 hours before biotin treatment for 45 min, followed by streptavidin pull-down for biotin-labelled proteins. After MS/MS analysis, we identified 768 proteins with at least a 2-fold enrichment by A4mTBYN compared with mTBYN, including 362 proteins exclusively labelled by A4mTBYN. Since we suspect that ADF may interact with transcriptional machinery, we filtered the candidates to systemically defined TFs (Tian et al. 2020) and found 67 TF enriched by A4mTBYN, including 39 exclusive candidates (Fig 3F, H). Among those TFs, members of the WRKY family were of immediate interest, as WRKYs are generally stress-related (including pathogen interaction) TFs exclusively existing in plant species (Javed and Gao 2023). This line of experimentation is in support of our working hypothesis that WRKY TFs may co-function with ADFs in immune signaling events.

Indeed, we identified 3 exclusively labelled, and a total of 8, WRKYs specifically enriched by A4mTBYN (Fig 3F, I). At this point, we hypothesized that ADF4, as a representative of class I ADF, has considerable affinity to interact with TFs, including WRKYs, to possibly co-regulate plant immunity. In addition to the identified interaction(s) with defense-associated TFs, we further hypothesized that histone and associated proteins are also likely involved in ADF transcriptional regulatory mechanism in plant. This is supported by a study in humans that suggested that *Hs*Drebrin can interacts with histone reader ZMYND8 – through its ADF-H domain – to competitively inhibit its interaction with histone (Yao et al. 2017). In support of this, we found evidence of 23 histones and associated proteins being enriched by A4mTBYN (Fig. 3F, J). This suggests that ADF may interact with histone complexes and regulate transcription via a histone-based epigenetic mechanism as well. Details of the enriched proteins are provided as Supplemental Material 1.

ADF2/3/4 specifically interact with WRKYs

Given the importance of WRKYs in plant immunity (Javed and Gao 2023), we assume that the potential of ADF-WRKY interaction revealed by TurboID proteomics implies a pro-immune transcriptional regulatory mechanism involved with nuclear ADFs. However, because Arabidopsis has 11 ADFs (Fig. 1A) and 74 WRKYs (Li et al. 2020) serving diverse functions, plus 12 ACTs (McDowell et al. 1996) possibly involved into the complex due to the nature of ADF, it is difficult to study them as an entire group. In order to further clarify the molecular function of ADF-WRKY interaction, we developed strategies to select appropriate representative candidates to describe this interaction.

First, we analyzed the aforementioned mRNA-seq datasets of PTI and ETI transcriptome (Fig. 1B) to determine the expression profile of all WRKYs (supp. Fig. 2-3). We found that all WRKYs showed low expression levels in leaves at the naive, resting state (i.e., without immune elicitation); however, during immune signaling, dozens of WRKYs are boosted, suggesting their involvement in immunity and potential relationship with ADFs participated in this process. Next, we used two principles to further screen-down the WRKY candidates: (1) all clades in WRKY family should be covered and (2) WRKYs reported to be associated with immunity and/or pulled-down by our TurboID (Fig. 2I) are prioritized. In such manner, we finalized 16 WRKY candidates covering 8 phylogenic groups, as summarized in Fig. 3A.

To determine which among these WRKYs mediate specific interaction with ADF, we conducted semi-quantitative BiFC to evaluate the interaction intensity of each WRKY candidate with ADF4. nY-ADF4 and cY-WRKY were co-transformed into Col-0 protoplasts to measure their overall fluorescence level using image computational approaches. As shown in Fig. 3B, half of the WRKY candidates showed detectable interaction intensity (descending group greater than “e”) with ADF4, while their interaction intensities had contrast variation. Among the candidates, WRKY22/29/48 were the strongest interactors, and WRKY6/8/18/28/33 were medium-weak interactors. Interestingly, these interactors concentrated in group Ib and IId, indicating the specificity of ADF-WRKY interaction may be related to structural features of these clades. In a further localization assay, we verified that ADF4 co-localized with WRKY29/48 in the nucleus (Fig 3C), and their BiFC signal majorly distributed in the nucleus (Fig. 3D) as well, in accordance with their subcellular localization. Besides, a DC3000 growth assay using *wrky22/29/48* triple mutant suggested that these WRKYs are indeed significant for plant immunity (Fig. 3G). Herein, we choose WRKY29 and WRKY48 as primary and secondary representative of the study, respectively.

Next, to understand the interaction specificity among all leaf-expressed ADFs, we conducted BiFC on ADF1-6 in combination with WRKY29/48 and 40 (as negative control). As shown in Fig. 3E, ADF2/3/4 showed strong interaction with WRKY29/48 and no interaction with WRKY40. Besides, ADF6 was a medium interactor; ADF1 was a weak interactor; ADF5 was a non-interactor. Since ADF1/2/3/4/6 displayed a similar interaction pattern with WRKY29/48, it is deducible that WRKYs' interaction with these ADFs may rely on a similar mechanism. Assuming ADFs have similar redundant functions, we choose ADF4 as a representative in the following studies.

To understand whether the ADF-WRKY interaction depends on simultaneous ADF-ACT interaction to rigorously form a WRKY-ADF-ACT triplex, we introduced a novel ADF4 mutant, ADF4_R98A/K100A, referring to previous studies (Du et al. 2016; Tanaka et al. 2018). Deduced from 3D structure, this mutant is unable to interact with ACT because the two mutated residues disrupted an alpha-helix on ACT-ADF interaction interface. Hence, we named this mutant ADF4$^{d\alpha3}$ (for "disrupted alpha-helix III") and found that ADF4$^{d\alpha3}$ indeed cannot bind to actin filament like general ADFs (supp. Fig. 4). Surprisingly, ADF4$^{d\alpha3}$ can still interact with WRKYs at high intensity, indicating the ADF-WRKY interaction *per se* does not necessarily require ACT as a scaffold. Previous studies reported that immune-triggered ADF phosphorylation on ADF-ACT interface prohibits this interaction to mediate actin remodeling (Dong and Hong 2013; Lu et al. 2020). Since ADF-WRKY and ADF-ACT interactions potentially use different interfaces, such phosphorylation may render different impact to ADF-WRKY interactions. Therefore, we conducted a BiFC assay using several ADF phosphomimic mutants and learned that these phosphorylation events do not substantially inhibit ADF4-WRKY29 interaction (supp. Fig. 5). On the contrary, S6D and S105D mutation on ADF4, which dissociates it from actin, generates slightly higher interaction intensity. These results implied that ADF-WRKY and ADF-ACT are relatively independent processes, and phosphorylation inhibiting ADF-ACT interaction may push the equilibrium of ADF-ACT and ADF-WRKY complex to the WRKY side, representing a nuclear phase of ADF functionality.

To further verify the physical interaction of ADF and WRKY using an alternative approach, we conducted a co-immunoprecipitation (co-IP) assays. Initially, we co-expressed FLAG-WRKY29 or WRKY29-FLAG together with wild-type ADF4-HA in *Nicotiana benthamiana*; this approach did not identify a strong ADF4 enrichment by α-FLAG IP (data not shown). Given that most ADF4 present within the cell may locate in the cytoplasm, and that actin may compete with WRKY29 for interaction, we improved the strategy by using ADF4_S6D/dα3-NLS (abbr. ADF4^{DdN}/A4^{DdN}) as an alternative. As mentioned above, S6D may enhance ADF-WRKY interaction intensity; dα3 can inhibit ADF4-ACT interaction to eliminate actin competition. The additional NLS tag serves to enhance the nuclear entrance to further increase the possibility to interact with nuclear proteins. With this mutant, we demonstrated that ADF4 indeed interacts with WRKY29 *in vitro* (Fig. 3F). Interestingly, FLAG-WRKY29 exclusively interacts with an unknown post-translational modification product of A4^{DdN} but not non-modified protein variants. However, we are uncertain whether this modification also exist in Arabidopsis rather than an artifact due to *N. benthamiana* overexpression. Besides, WRKY29-FLAG did not show A4^{DdN} affinity like FLAG-WRKY29, potentially because a c-terminal cleavage product in *N. benthamiana* without ADF4 interaction capability competes with full-length WRKY29 during protein isolation and co-immunoprecipitation.

N-terminal sequence of ADF regulates ADF-WRKY interaction

One key piece of data, presented above, further raised our interest as we continue test our hypotheses: ADF2/3/4, but not ADF1, displayed strong WRKY interaction, but ADF1 has the closest phylogenic relationship with ADF4 (Fig. 1A, 3E). By comparing their sequences, we realized that such paradox may result from their different N-terminal sequence that is not reflected in the phylogenic tree, because those ADFs were defined by different representative splicing models. Alternative splicing exists in Arabidopsis ADF family and modifies their N-terminal overhang. The representative model ADF1.2 has an additional 11 residue overhang (namely N1.2) on the N-terminal compared to the representative model ADF4.1 (Fig. 3H). Therefore, as the representative models were used by default, the low BiFC intensity of ADF1(.2) might suggest a potential inhibitory function of ADF N-terminal sequence. To test this hypothesis, we measured WRKY interactions of different splicing products of ADF1/4 as well as their chimeras. As shown in Fig. 3H, I, ADF1.1 (the isoform without N1.2), ADF4.1, and ADF4.2 have similar high affinity to WRKY29, while ADF1.2 was low as expected. Further, when N1.2 was fused to ADF4.1, it is no longer able to interact with WRKY29 at high affinity, suggesting that N1.2 indeed inhibits ADF-WRKY interaction. However, an alternative explanation may exist as N1.2 are structurally rigid

267 and increases the distance between nY and cY to bind each other. To inspect this possibility, we tested N5.1-ADF4.2
268 chimera using N-terminal sequence of ADF5.1, which is only 4 residues longer than ADF4.1. As a result, it displayed
269 low WRKY interaction, indicating it is the sequence and structure, rather than length of the ADF N-terminal overhang,
270 that regulates ADF-WRKY interaction. Hence, it is deducible that the alternative splicing of ADFs may be functionally
271 related to the equilibrium of their cytosolic-nuclear activity.
272
273 **ADF-WRKY and HsDrebrin-ZMYND8 have different interaction interfaces**
274 Since *Hs*Drebrin can use its ADF-H domain to bind the histone reader ZMYND8 as a potential transcription regulatory
275 mechanism, we were curious whether the ADF-WRKY interaction in Arabidopsis also utilizes the same interface. To
276 answer this question, we expressed the truncated *Hs*Drebrin ADF-H domain (*Hs*DAH) in our BiFC system and found
277 that *Hs*DAH had a lower, yet still robust, interaction with WRKY29 (Fig. 3J). When we introduced single or quadruple
278 mutations of *Hs*DAH on the HsDrebrin-ZMYND8 interface (Yao et al. 2017), the interaction intensity was not
279 substantially changed (Fig. 3J). These results indicated that ADF-WRKY and HsDrebrin-ZMYND8 likely do not share
280 similar interaction interfaces.
281
282 **ADFs interact with WRKY-DNA complex**
283 WRKYs regulate transcription through binding to the W-box motif ((T)TGAC(C/T)) in promoter sequences of stress-
284 responsive genes (Jiang et al., 2017a). Considering ADF-WRKY interaction, it is reasonable to inspect whether ADF is
285 involved in transcriptional regulation as a component of the WRKY-DNA complex. To answer this question, we
286 conducted a chromatin immunoprecipitation (ChIP) experiment using *adf4/wrky29* double mutant protoplast co-
287 expressing ADF4-HA and/or WRKY29-MYC (Fig. 4A). So far, there has been no published genomic study identifying
288 promoters targeted by WRKY29. To establish a testing system, we presumed that WRKY29 can regulate its own
289 promoter in a similar pattern to the previously studied case of WRKY18/40/60 (Liu et al., 2012). Accordingly, we found
290 5 W-boxes (see Fig. 4B) on WRKY29 promoter (pW29; -1900 to +1). Additionally, a study over BAG7, an ER-nuclear co-
291 chaperone involved in unfolded protein response, revealed that WRKY29 can bind the W-boxes of pBAG7 (Li et al.,
292 2017b). Therefore, we measured the pull-down fraction containing the W-boxes in pW29 and pBAG7 from different ChIP
293 combinations through qPCR.
294
295 As shown in Fig. 4C, all W-boxes containing fractions in pW29 were enriched by ChIP of WRKY29-MYC, suggesting
296 WRKY29 indeed binds to the W-boxes as a typical TF in WRKY family. Interestingly, when co-expressing WRKY29-Myc
297 and ADF4-HA, both α-HA and α-Myc ChIP were able to significantly enrich the pW29 W-box fractions, which indicated
298 that WRKY29 and ADF4 not only bind to each other but also form a complex together with their targeted DNA. In addition,
299 because pro-immune transcription requires specific immune elicitors, we also introduced the treatment of flg22 as a
300 variable. However, the impact of flg22 was not obvious, indicating PTI is not a prerequisite to trigger the ADF4-WRKY29-
301 DNA interaction at the experiment condition. However, we cannot exclude the possibility that their interactive affinity
302 can be enhanced by any immune signaling when ADF4 and WRKY29 are not overexpressed as experiment setting.
303 Another potential target of WRKY29, pBAG7, was also enriched by WRKY29 and ADF4 with minor amplitude, suggesting
304 the W-box affiliation of pBAG7 was not as strong as pW29 in the experimental condition.
305
306 **ADF2/3/4 enhance the WRKY29-mediated transcriptional activation**
307 As ADF-WRKY interaction occurs on the promoters targeted by WRKY, we are curious whether such interaction can
308 regulate the activity of WRKYs. To test this, we constructed a promoter reporter system to quantify the activity of WRKY
309 in the presence/absence of ADFs. The reporter system is comprised of 3 vectors, which contains p35S::WRKY-BFP
310 (mTagBFP), p35S::ADF-RFP (mCherry), and GFP (mEGFP) driven by WRKY-targeted promoter, respectively (see Fig. 4D).
311 When the GFP reporter vector is co-transformed with the combinations of WRKY-BFP and/or ADF-RFP into protoplasts,
312 all three fluorescence signals can be quantitatively measured by large-scale confocal microscopy, and therefore the
313 differentiated levels of GFP can be explained by different transcriptional activation amplitude by WRKYs and/or ADFs.
314 pW29 and pBAG7 are tested for WRKY29; at the same time, pW48 (assumed as auto-regulated by WRKY48) and pW46
315 (Gao et al., 2013) are used to test WRKY48. Null mutant *wrky29* and *wrky48* were used as the source of protoplast to
316 eliminate the background WRKYs that were unmeasurable. As expected, both WRKY29 and WRKY48 were able to boost
317 the expression of their targeted promoters; more importantly, ADF4 further enhance the transcription activation
318 amplitude when co-transformed with WRKY29 (Fig. 4E).
319

Next, we tested which of the leaf-expressed ADFs can enhance WRKY activity. In addition to ADF1-6, we also introduced ADF4-NLS and ADF4-NES (nuclear export signal) to evaluate the differential contribution of ADF-mediated transcriptional regulation by ADFs as a function of nuclear and cytoplasmic localization. As shown in Fig. 4E, ADF2/3/4 indeed boosted the activity of WRKY29, while ADF1 and ADF5 did not exhibit such an impact. At the same time, the ADF4-NLS led to the highest expression level among all the groups, which fully supports the hypothesis that ADFs enhance WRKY's activity by binding WRKY at the targeted promoters inside the nucleus. Perplexingly, ADF4-NES also showed a relatively high reporter signal, similar to that observed for ADF4. By further computational analysis, we found that this was a potential artifact related to varied ADF/WRKY expression levels, as the normalized impact of per unit of ADF4-NES was very low (supp. Fig. 6). Additionally, ADF4$^{d\alpha3}$ was also able to enhance the activity of WRKY29 to a level identical to ADF4 (Fig. 4E), confirming that the WRKY boosting effect does not require the simultaneous interaction with actin. The sum of these data mirrored the BiFC results (Fig. 3E), suggesting that strong WRKY interactors – ADF2/3/4 – also enhance the activity of WRKYs, which serves as a potential mechanism for ADF to regulate plant immunity in the nucleus.

ADF4, binding WRKY29, targets immune genes genome-widely and regulates WRKY29 targeting affinity and spectrum

Since our study revealed ADFs as a WRKY regulator, our next major question is how ADF's WRKY binding and regulatory activity can contribute to plant immunity. Therefore, we conducted a set of ChIP-seq experiments to learn what the function of WRKY29 is as a TF and how ADF4 is involved when forming the complex. In brief, we transformed different combinations ADF4-HA and WRKY29-Myc to *wrky29/adf4* protoplast to pull-down ADF- and WRKY-bound genome fractions (Fig. 5A, supp. material 2).

As the first study systematically revealing the targeting spectrum of WRKY29 *in planta*, our data confirmed that WRKY29 mostly bind to the promoter regions as a typical TF (Fig. 5B, C). Totally 4075 genes covering various immune pathways are targeted by WRKY29 (W29M, Fig. 5D, F), indicating that WRKY29 is indeed an immune-regulatory TF as we expected. Surprisingly, when ADF4 is transformed alone (A4H), it still targeted 612 genes that partially overlap with those of WRKY29 (Fig. 5D) and was also localized mainly on promoters (Fig. 5B, C). In terms of the biological function of the targets, A4H resembles the pattern of W29M, which focuses on SA-immunity related pathways, while the enrichment level and significance are not as high as W29M (Fig. 5F). Given that ADF4 does not have any DNA-binding domain, it was deducible that ADF4 potentially binds to other TFs or transcriptional machinery as a wide-functional transcriptional regulator.

When ADF4 and WRKY29 are co-transformed, several interesting alternations were observed on behaviors of both WRKY29 and ADF4. For WRKY29, ADF4 changed its targeting affinity and spectrum, as additional 687 new promoter loci were found yet 449 got lost (W29M vs A4W29M, Fig. 5B). To further increase the resolution to understand ADF4's regulatory impact, we performed a differential peak-calling analysis over individual peaks (splitting minor summits, Fig. 5E). We found that ADF4 significantly increased the enrichment level of single peaks covering 4454 genes while decreasing those of 288 genes with partial overlapping, suggesting that ADF4 majorly enhances or introduces additional promoter binding affinity of WRKY29.

For ADF4, on the other hand, the introduction of WRKY29 entirely changed and specified its targeting spectrum. First, WRKY29 enables ADF4 to interact with additional 2191 genes (Fig. 5D), with peaks of ~4700 genes showing significantly changed (mostly upregulated) enrichment level (Fig. 5E). Most of the enriched genes by A4W29H overlap with those by A4W29M/W29M (Fig. 5D) and share the same function (Fig. 5F). Since WRKY29, rather than ADF4, has a direct DNA binding structure, the acquired DNA binding spectrum of ADF4 should be introduced by the formation of ADF-WRKY complex. To further inspect this hypothesis, we performed a co-localization assay using the enrichment fold of overlapped genes from A4W29M and A4W29H (Fig. 5G). As A4W29W and A4W29H showed strong and significant linear correlation, we believe that the ADF-WRKY complex widely spread over the promoter loci across the genome. Combining previous results, we concluded that WRKYs, through physical interaction, can actively lead nuclear ADFs to a specific spectrum of promoters, and therefore introducing additional regulatory effect to immune genes beyond WRKY's activity *per se*.

Next, we conducted a *de novo* motif enrichment analysis using the peak-summit neighboring sequences to interrogate the biochemical features of the WRKY and ADF-WRKY complex while limiting the bias introduced by previous studies (Fig. 5H). As expected, we found that WRKY29 utilizes W-boxes as its theoretically targeted motif, yet might also integrate into larger complexes with other TFs, since binding motifs of other DNA binding protein families were enriched as well. For ADF4 without WRKY29, the enriched motifs reflected various families including C2C2 (family of *Hs*ZMYND8, a target of *Hs*Drebrin), MYB, HMG, and WRKY, suggesting that ADF extensively regulates other DNA-binding proteins beyond WRKYs. By introducing WRKY29 to ADF4, the motifs enriched by ADF4 altered back to a pattern resembling WRKY29, echoing our previous conclusion that WRKY29 guilds ADF4 to its own targeting spectrum to co-regulate resistance genes.

Nuclear and cytoplasmic ADF have different roles in plant immunity

Considering the revealed biochemical function of nuclear ADF, we are curious in whether and to what extent nuclear ADFs contribute to plant immunity. To address this question, we constructed complementation lines expressing ADF4 or ADF4-NES/NLS in *a234* background to restrict ADF4 within cytosol and nucleus and distinguish their different functions (Fig. 6A). As expected, ADF4-NES displayed very typical actin bundle localization in cytosol without nuclear signal, whereas ADF4-NLS was perfectly restricted within nucleus, and native ADF4 presented both (Fig. 6B, C).

To investigate how ADFs differentially contribute to plant immunity by different subcellular localization, we first tested their resistance against the model bacterial pathogen *P. syringae*. As shown in Fig. 6D, *a234*, which phenocopies *wrky22/29/48*, has dampened basal defense against DC3000. Interestingly, the *a234* phenotype was fully complemented by expressing native *ADF4*, partially complemented by ADF4-NLS, but not by ADF4-NES. Further, we posit that this phenotype potentially involves a dosage effect, as we found high- and low-expression lines have different resistance levels (supp. Fig. 7). When ETI against AvrPphB was used as the defense stimulus, the major profile of resistance was similar to that of wild-type DC3000; additionally, ADF4-NLS fully restored resistance (Fig. 6E). These results suggested that nuclear – rather than cytosolic – ADF drives the majority of resistance against DC3000, which is even more critical upon certain types of ETI.

To further this line of investigation, we tested whether ADF – especially its nuclear fractions – contributes to a larger variety of pathogens. Particularly, we chose *Pectobacterium carotovorum*, the pathogen of bacterial soft rot, as a representative of absolute necrotrophs and *Golovinomyces cichoracearum*, the fungal pathogen of powdery mildew, as a representative of absolute biotrophs. When *P. carotovorum* WWP14 was inoculated, we did not observe any significant difference between Col-0, *a234*, and wrky22*/29/48*. (Fig. 6F), potentially because ADF2/3/4 are not critically contributive to resistance against this pathogen at natural expression levels. However, lines overexpressing ADF4 are more susceptible to WWP14, indicating a potential dosage-dependent role of ADFs in this defense process. For powdery mildew infection, there is no significant difference in the fungal growth among different genotypes inoculated with *G. cichoracearum* UCSC1 (Fig. 6G, H). This observation shows an interesting discrepancy from the previous study that suggests an enhanced resistance against powdery mildew in *ADF1/2/3/4*-silenced line (Inada et al. 2016). However, it is noteworthy that their study uses a different powdery mildew species, *G. orontii*, which may explain the different phenotypes. Inspired by this hypothesis, we tested the *G. cichoracearum* UCSC1 growth on the same *ADF1/2/3/4*-silenced line, and rather than resistance, we observed contrast greater susceptibility compared to Col-0 (supp. Fig. 8), which suggests that ADF's roles in pathogenesis of different powdery mildew species can be substantially different.

Apart from typical model pathogens, we also investigated whether cytosolic and nuclear ADF influences the interaction with root commensal bacteria as a perspective from wilder concept of plant-microbe interaction. Such bacteria enter and proliferate in root apoplast and introduce stimuli regulating morphological development and immune maturation, while not causing disease. In our scheme, we started by measuring root growth upon different commensal bacteria treatment, as an index reflecting the degree of plant response commensal microbes (Fig. 6I). As a result, we indeed identified that *a234* showed a minor root zig-zag morphology and a more severe root growth inhibition upon several species of commensals, compared to Col-0 (Fig. 6J). Regarding this, we chose Arabidopsis rhizosphere *Pseudomonas sp*. KD5 (IMG ID: 2228664007, lab internal ID: "50") as a representative strain for further analysis. When "50" was inoculated onto different genotypes, there was no significant difference over bacterial growth rate (Fig. 6K). However, *a234* displayed stronger root growth inhibition following "50" treatment, which was not fully complemented by ADF4, although the ADF4-NES expression line was phenotypically more similar to Col-0 in terms of inhibition level. At the

same time, *wrky22/29/48* did not phenocopy *a234*, suggesting these WRKYs are not critically involved in root growth regulation by rhizosphere commensal bacteria. Combining current knowledge (García-González and van Gelderen 2021), we assume that ADF2/3, rather than ADF4, majorly contribute to root development in an actin-related manner that resembles the roles of ADF4 in hypocotyl development (Yu et al. 2025).

In summary, the cytosolic and nuclear function of ADF in immunity varies among different types of pathogens. ADFs, especially their nuclear fraction, contribute to basal defense and at least certain types of ETI against *P. syringae*. However, they do not impact defense against *P. carotovorum* WWP14 and *G. cichoracearum* UCSC1 at natural expression level, but ADF4 overexpression potentially increases the susceptibility to WWP14. Besides, ADFs are also involved in root morphogenesis regulated by commensal bacteria, which may be majorly related to ADF2/3 instead of ADF4. These results indicate that the cytoplasmic-nuclear function of ADF is relatively complex across different types of plant-microbe interaction.

Nuclear ADFs regulate transcriptome at the resting state and immune events

Since nuclear ADFs contribute to plant immunity potentially via regulating transcription machinery as provided above, we further conducted a series of mRNA-seq experiments to elucidate their regulatory impact and immune function in detail. In our scheme, samples from Col-0, *a234*, and ADF4/NES/NLS complementation lines, with mock or PAMP (flg22+elf18 mixture) treatment, are collected and sequenced to quantify the transcriptome at the resting state and immune (PTI) events, respectively. While the primary variable influencing the transcriptome is PAMP treatment, significant and massive differences across genotypes are substantially obvious (Fig. 7B, supp. Fig. 9). In total, we identified 4389 deferentially expressed genes (DEGs) among all genotypes (supp. material 3), revealing the significance of nuclear ADFs.

First, compared to *a234*, Col-0 has ~1500 DEGs at the resting state (i.e., mock treatment) and ~900 DEGs upon PTI (Fig. 7C), which controls various physiological processes including immunity, defense hormone signaling, cytoskeleton organization, and other cellular and (Fig. 7D). At the same time, *a234*/A4 perfectly phenocopies Col-0 when compared with *a234* and Col-0. Therefore, ADF2/3/4 indeed significantly contributes to the expression of defense and development genes with certain levels of function redundancy. Second, complementing ADF4-NLS (*a234*/A4-NLS) dramatically changed the transcriptome pattern of *a234* by ~2000 DEGs over resting state and ~1000 DEGs upon PTI, whereas *a234*/A4-NES was almost identical to *a234*, which, echoing results above, substantially validated that nuclear – not cytosolic – ADFs possess the major transcriptional regulatory activity *in planta*. Third, nuclear ADFs regulate partially different genes and biological pathways at resting state and immune events. As shown in Fig. 7D, (nuclear) ADF4 in naïve plants mainly regulates growth-related metabolism, cytoskeleton organization, general immune signaling, and DNA processes. However, when PTI is triggered, DEGs shift to focus on immune-related glucosinolate metabolic processes, hormone (e.g., auxin, SA, JA, ABA) signaling, and cell communication. Therefore, nuclear ADFs regulate different groups of genes at different statuses of the growth-defense equilibrium.

Regarding the ADF-WRKY coregulatory mechanism revealed by this study, we proceeded to inquire whether – or to what extent – the molecular function of ADF4-WRKY29 complex can explain the dampened immune transcriptome due to the lack of ADFs. We compared all DEGs revealed from between col-0, *a234*, and *a234*/A4-NLS, with ADF4 targeted genes identified through ChIP (Fig. 7E). As expected, we indeed find 342 genes both regulated by ADFs at expression level and physically targeted by ADF4 on their promoters. However, the majority of the DEGs or ADF4 targeted genes do not overlap, indicating that the co-regulation on promoters by the ADF-WRKY complex – at least by merely ADF4 and WRKY29 – may not fully explain the transcriptional functionality of ADFs. As a further annotation to the nuclear activity of ADFs, our categorical analysis suggested that ADFs regulates the expression level of 309 TFs, covering 39 TF families beyond WRKY (Fig. 7F). Considering that nuclear ADF4 has specific affinity to 67 TFs through TurboID (Fig. 2H), we propose that ADFs mediate a broad spectrum of transcriptional regulation potentially by directly interacting with certain TFs to regulate their activity, which influences the expression level of more TFs through their inter-regulatory network, thereby facilitating immune maturation and defense. At the same time, while this activity may be dispensable to actin-ADF interaction, we cannot totally exclude the possibility that ADF's nuclear function may be related to its actin interaction activity (e.g., recruiting actin filament to transcriptional machinery). Therefore, nuclear ADFs potentially have multiple layers of function regarding transcriptional regulation, where those related to ADF-WRKY complex represent one of the typical cases.

Discussion

Plant immune activation mobilizes the cytoskeleton, including its associated proteins, to transport and stabilize defense molecules and organelle, as well as numerous additional physiological responses (e.g., pathogen triggered stomatal closure). Due to the significant roles of cytoskeleton remodeling in plant immunity, it is reasonable to deduce that critical proteins directly regulating cytoskeletal dynamics are indispensable for plants to render full strength of immune response. Massive experimental evidence matches this theory (Li and Day 2019), making it a popular mechanism model to explain why actin remodelers, such as ADFs, influence pathogen susceptibility and resistance. However, since this process is theoretically happening in the cytosol, the canonic function of ADF cannot explain why ADF evolved to bring actin into nucleus (Dopie et al. 2012). Moreover, it is unclear how nuclear-localized ADFs contributes to certain types of resistance (Inada et al. 2016), which implies a different type of moonlighting function currently undescribed.

In this study, we used the CRISPR-Cas system to eliminate the redundancy of Arabidopsis leaf-expressed ADFs, successfully defining the nuclear-exclusive function of ADF4, as a representative of Class I ADF, in plant immunity. As an explanatory mechanism, we identified WRKY22/29/48 as strong interactors of ADF2/3/4, providing evidence that these interactions regulate the promoter activity and targeting spectrum of WRKYs. Through this study, we propose a novel perspective to review the role of ADF proteins in plant immunity and beyond – a function that is relatively independent from its traditional identity as a regulator of actin remodeling. Here, we would like to discuss the significance, potential, uncertainty, and limitations of the newly identified transcriptional regulatory function of ADF.

As illustrated in Figure 8, we summarized the discoveries and supported hypotheses for an integrated cytoplasmic-nuclear functional model of actin and ADF. Our study, combined with previous work in this field, note that a full/robust immune requires ADF to have both actin severing/depolymerization activity within cytosol and transcriptional regulation activity in the nucleus, integratively. As seemingly straightforward as this activity may appear, this integrated dual-phase function is more complex. As previously noted, immune signaling can activate upstream kinases capable of phosphorylating corresponding ADFs (Zhao et al. 2016; Lu et al. 2020). When ADF is phosphorylated (e.g., S6 and S105 of ADF4, or S3 of *Hs*CFL), it will dissociate from actin, thus eliminating the traditional role of ADF as a actin depolymerization factor, which is regarded as a central mechanism to regulate actin architecture, and including immune-triggered actin remodeling. As presented herein, ADF-ACT and ADF-WRKY interactions do not share interfaces on ADF (Fig 3E, F; Supplemental Fig. 4), so we posit that ADF phosphorylation events decrease the ADF-ACT interaction intensity and hypothetically increase the ADF-WRKY interaction intensity. At present, we still do not know if phosphor-regulation either directly enhances the binding affinity between ADF and WRKYs, or if this is an indirect influence whereby phosphorylation promotes ADFs disassociation from ACTs, which in turn drives the ADF competition equilibrium to ADF-WRKY. If any of these mechanisms are valid, it indicates that ADF-ACT and ADF-WRKY interaction reflect two potential antagonistic aspects of ADF function. To fully test this hypothesis, a detailed dynamic phosphorylation profile of ADF during immune process *in vivo* is necessary, as well as a comprehensive analysis of ADF nuclear shuttling speed of different phosphorylation variants. We assert that these are critical questions to be addressed to fully define the ADF phospho-switch hypothesis.

ADF2/3/ 4 are critical for full-strength pro-immune transcription (Fig. 7) and resistance against DC3000 (Fig. 1E-H, 6D-E), a response in which case the nuclear – rather than cytosolic – action of ADF is required. Combined with ADF2/3/4's ability to interact with WRKY22/29/48 and the results suggesting *wrky22/29/48* phenocopies *a234*, we conclude that the ADF-WRKY interaction can explain the immune phenotypes related to nuclear ADFs. However, as noted in the TurboID data, there were additional ADF4-interacting TFs from other families beyond WRKY, as well as histones, histone readers, and modifiers (Fig. 2H, J). Correspondingly, the motif enrichment analysis using ChIP-seq reads enriched by ADF4 also discovered many cis-element patterns not related to the WRKY family. Hence, we infer that nuclear ADFs are potentially involved in multiple intertwined fractions of the transcriptional regulatory machinery, and that the ADF-WRKY interaction may be just the tip of the iceberg.

It is noteworthy that the DEG analysis identified that nuclear ADF4 also controls biological pathways related to development, metabolism, and DNA-related processes during the non-elicited (i.e., in the absence of pathogen infection) resting state. Combined with recent studies suggesting that ADFs regulate nuclear organization (Matsumoto

et al. 2023) and senescence (Matsumoto et al. 2024), it is reasonable to deduce that nuclear ADFs have more general transcriptional regulatory functions beyond immunity, potentially by regulating other TFs or histone-based epigenetics. At the same time, such a mechanism potentially has a broader scope of application beyond Arabidopsis – or even plants. As the ADF/cofilin family is widespread across almost all eukaryotic kingdoms that uses actin in any cellular process (Chen and Day 2024), it is expectable that ADFs may play similar roles in transcriptional regulation in other plant and animal species, including human. Currently, there are many clinical diseases associated with dysfunctional ADFs/cofilins that exhibit abnormal transcriptome pattern (Shehjar et al. 2024; Xing et al. 2024), but this is stereotypically considered as an impact of abnormal or pathological actin dynamics. As for plant disease in model and crop species, most evidence remains at genetic level (Li and Day 2019), leaving greater intellectual challenges to rationalize how genotypes related to ADFs contribute to phenotypes in pathogenesis and immunity at cellular and molecular level. However, as we proved that ADFs can mediate immune and general transcriptional regulation through interaction with TFs, which is not necessarily related to ADF-ACT interaction, the cytosolic and nuclear ADF functionality is conceptually deconstructed into two relatively independent, but continuously inter-communicating, signaling nodules. Hence, we hope this study can provide the community with a novel perspective to explore the roles of ADFs in plant and human disease, as well as issues in general biology.

Materials and Methods

Plant and microbe materials

All plants were grown in a BioChambers model FLX-37 walk-in growth chamber (BioChambers, Manitoba, Canada) at 20 °C with 12h light/12 dark with 60% relative humidity and a light intensity of 120 µmol photons $m^{-2} s^{-1}$.
Arabidopsis mutant *adf1* (Salk_144459), *adf3* (SALK_139265), *wkry22* (CS68112), *wrky29* (CS339192), and *wrky48* (SALK_066438) were purchased from ABRC and screened for homozygosity. *adf4-2* (SALK_121647) were generously provided by Dr. Yan Guo. We identified that *adf4-2* contains another insertion in *AT1G77500*, so the original *adf4-2* was further screened to eliminate *at1g77500*. To further clean other potential insertions, *adf4-2/AT1G77500(WT)* was then backcrossed to Col-0 to obtain a purified *adf4-2* line, namely *adf4-2b*. The construction strategy and genotyping of all *ADF* and *WRKY* high order mutants are described in Fig. 1D and/or Supplemental Fig. 1.

Pseudomonas. *syringae* pv. tomato DC3000 and its AvrPphB-containing strains are preserved stocks of the Day Lab, Michigan State University (MSU), as previously described (Lu et al. 2020). *Pectobacterium carotovorum* WWP14 was generously gifted by Dr. Greg Howe (MSU). *Golovinomyces cichoracearum* UCSC1 is historically preserved in the Xiao Lab, University of Maryland, as previously described (Wu et al. 2024). Arabidopsis root commensal bacterial strains are preserved stocks of the Lebeis Lab, MSU. Strain identities as follows. WCS417: *Pseudomonas simiae* sp., IMG ID 2585427642; 50: *Pseudomonas sp*. KD5, IMG ID 2228664007; CL58, *Pseudomonas umsongensis* UNC430C58Col, IMG ID 2556921015; 36: *Pseudomonas mandelii* 36MFCvi1.1, IMG ID 2521172653.

Construction of plasmid vectors

TurboID, BiFC, ChIP, promoter assay, and *ADF4* complementation in this study are enabled by newly constructed plasmid vectors, described as supp. material 4. Related primers are listed in supp. material 5.

CRISPR gene editing

gDNAs targeting *ADF2* and *ADF4* were designed using CRISPR-P, as described in Supplemental Table 1. gDNAs were inserted into CRISPR-Cas9 vector psgR-Cas9-At (Mao et al. 2013) followed by insertion into pCAMBIA1300. Resultant constructs were then transformed into Col-0 and *adf3*, to knock out *ADF2* and *ADF4*, respectively, generating *adf2* and *adf3/4*. T1 antibiotic-resistance positive plants with chimeric polymorphism on targeted loci were selected; T2 plants with homozygous null mutation on targeted loci and without CRISPR vector insertion were selected for further experiments.

Co-immunoprecipitation

Co-immunoprecipitation (co-IP) assays were performed based on a protocol adapted from (Lu et al. 2020), with slight modifications. In brief, ten *N. benthamiana* leaf discs (1 cm diameter) were harvested and frozen into liquid nitrogen. Leaf lysates were prepared by grinding leaf discs in liquid nitrogen and then grinded with 5mL homogenization buffer (50 mM Tris, pH 7.4, 150 mM NaCl, 10% glycerol, 0.2% triton X-100, 1mM DTT, 1 x cOmplete™ Protease Inhibitor

584 Cocktail (Sigma #04693116001), and 1mM PMSF). Homogenized samples were sonicated at 12% amplitude for a total
585 of 30s using a needle sonicator to release nuclear proteins and then centrifuged at 4 °C at 18600g for 5 min. 4 mL of the
586 supernatant in a microcentrifuge tube was slowly rotated at 4°C for 4h with Pierce™ Anti-DYKDDDDK Magnetic Agarose
587 (Thermo #A36797) following the manufacturer's instructions. Samples – associated with magnetic agarose – were
588 washed using homogenization buffer for at least 3 times, 5 min each. For western blot analysis, enriched fractions -
589 beads with pulled-down fractions are mildly denatured by incubation with 1x LDS Sample Buffer (Thermo #B0008) and
590 50mM DTT at 70°C for 10min.
591
592 **TurboID and LC/MS/MS analysis**
593 Arabidopsis TurboID protocol was adapted from a previous study (Mair et al. 2019). Briefly, 10 Arabidopsis leaves were
594 first injected with a mixture of 1 μM flg22 and 1 μM elf18 or water as mock. Three hours later, the leaves were injected
595 with 50 μM biotin and treated for 1 hour before frozen in liquid nitrogen. Frozen leaves were processed through a typical
596 co-IP procedure as described above, except that an additional PD-10 desalting column (Cytiva #17085101) was used
597 to eliminate the residual biotin in the centrifuged leaf lysate supernatant following the official protocol. Pierce™
598 Streptavidin Magnetic Beads (Thermo #88816) is used for pull-down biotin-labeled proteins.
599
600 For proteomics, the streptavidin beads binding TurboID targeted proteome were washed by 50 mM ammonium
601 biocarbonate for 3 times. Trypsin, in the same buffer, was then added to the beads at 5 ng/μL so that the beads were
602 just submerged in digestion buffer and allowed to incubate at 37°C for 6 hours. The solution was acidified to 1% with
603 trifluoroacetic acid and centrifuged at 14000g. Peptide supernatant was removed and concentrated by solid phase
604 extraction using StageTips1. Purified peptides eluates were dried by vacuum centrifugation and frozen at -20°C or re-
605 suspended in 2% acetonitrile/0.1%TFA to 20 μL.
606
607 An injection of 5 uL was automatically made using a Thermo EASYnLC 1200 onto a Thermo Acclaim PepMap RSLC 0.1
608 mm x 20 mm C18 trapping column and washed for 5 min with buffer A (99.9% water/0.1% formic acid). Bound peptides
609 were then eluted over 35 min onto a Thermo Acclaim PepMap RSLC 0.075mm x 500mm resolving column with a
610 gradient of 8% buffer B (80% acetonitrile/0.1% formic acid/19.9% water) to 40% buffer B in 24 min. After the gradient
611 the column was washed with 90% buffer B for 10 min at a constant flow rate of 300nl/min. Column temperature was
612 maintained at a constant temperature of 50°C using an integrated column oven (PRSO-V2, Sonation GmbH, Biberach,
613 Germany). Eluted peptides were sprayed into a ThermoScientific Q-Exactive HF-X mass spectrometer using a FlexSpray
614 spray ion source. Survey scans were taken in the Orbi trap (60000 resolution, determined at m/z 200) and the top 15
615 ions in each survey scan are then subjected to automatic higher energy collision induced dissociation (HCD) with
616 fragment spectra acquired at a resolution of 15,000.
617
618 **Bacterial and fungal pathogen growth assay**
619 *P. syringae* inoculation and growth measurement was previously described (Lu et al. 2020). Briefly, DC3000 or
620 DC3000/AvrPphB in 10 mM $MgCl_2$ at OD_{600} = 0.002 (2e5 CFU mL^{-1}) was carefully inoculated to 5-week-old Arabidopsis
621 leaf with a blunt syringe. Plants were held at growth conditions with a transparent plastic dome. Leaves are harvested
622 at 2 days post inoculation (dpi). Twelve independent leaf disks with 4 mm diameter were collected and pooled as one
623 sample (biological repeat). If not specially claimed, each experiment uses 4 samples.
624
625 *P. carotovorum* WWP14 was grown in Luria Bertani (LB) media. Five μL of WWP14 solution in 10 mM $MgCl_2$ at OD_{600} =
626 0.02 was dropped on the center of one side of the main vein of 5-week-old Arabidopsis leaves. Plants were held at
627 growth conditions with a sealed transparent plastic dome. The major/minor axis of the infection plague, assumed as
628 an ellipse, were measured by a vernier caliper at 16-24 hours post inoculation (hpi) to determine the plaque area.
629
630 *G. cichoracearum* UCSC1 preservation and inoculation method was previously described (Wu et al. 2024). In brief,
631 UCSC1 was maintained on the Arabidopsis *eds1* mutant. Spores from 15~20 heavily infected *eds1* rosette leaves were
632 evenly spread on 24.5 x 10 inches, and a 48 μm mesh was used to gently brush the inoculum into the leaf. Plants were
633 kept in an inoculation chamber for disease development. For spore counting, 2-3 maximumly extended rosette leaves
634 at ~8 dpi were collected. Spores were suspended in 0.02% Silwet L-77 plus 0.02% Tween-20 and counted using a
635 LUNA™ Automated Cell Counter. For imaging of infected leaves, plants at ~10 dpi were used.

636
637 **Root commensal bacterial infection vertical plate assay (VPA)**
638 Seeds were surface sterilized by washing with 70% ethanol + 0.01% Triton-X for 3 minutes and then 10% bleach solution
639 for 5 minutes. The seeds were next washed 4 times with sterile DI water, 1 minute each. Sterilized seeds were kept in
640 the dark at 4 °C for 3 days and grown on ½-Murashige and Skoog (MS) plate for 7 days under growth condition. Seedlings
641 were then carefully transferred to ¼-MS plate previously spread with 150 µL bacteria (OD_{600} = 0.01) and set vertically in
642 growth condition; distance between seedlings is more than 2cm. Positions of the vertical plates were rearranged every
643 2 days to avoid impacts of light direction. Roots architectures are imaged using a scanner at 10 dpi. To count the
644 colonized internal bacteria, seedlings from vertical plates were carefully washed three times with PBS buffer and
645 weighed before homogenization using sterile glass beads in 1 mL sterile PBS for bacteria counting.
646
647 **Agrobacteria-based transformation**
648 The method for transient expression in *N. benthamiana* was previously described (Lu et al. 2020). Briefly, *A.*
649 *tumefaciens* GV3101 strains harboring expression constructs were pre-incubated at room temperature in induction
650 media (10 mM MES [pH 5.6], 10 mM $MgCl_2$, 150 mM acetosyringone) for 2 h before hand-infiltration into 5-week-old *N.*
651 *benthamiana* leaves using a 1-mL needleless syringe. Inoculated plants were kept in growth condition. Transformed
652 leaves at 2 dpi were used in downstream studies.
653
654 For Arabidopsis floral-dip, Agrobacteria were inoculated into 10 mL LB media with proper antibiotics overnight. After
655 centrifuge, the bacteria are re-suspended in 2 mL of the floral-dip buffer (1/2-MS, 5% sucrose, and 0.02% Silwet L-77).
656 Each flower to be transformed is dipped up-and-down for 10s. The plants with dipped flower are shaded in full darkness
657 with saturated humidity for 24 h and restore to growth condition for harvest.
658
659 **Arabidopsis protoplast transformation**
660 Arabidopsis protoplast preparation method is integrated from previous publications (Yoo et al. 2007; Wu et al. 2009)
661 with optimization presented as follows. In brief, leaf #8/9/10 from 5-week-old Arabidopsis plants were excised and the
662 lower epidermis of each leaf was removed using Scotch tape. The leaves were digested in the enzyme solution for 1.5h.
663 The obtained protoplast was washed in W5 solution, followed by resuspension in MMG solution at a cell concentration
664 of $5x10^5$ protoplast/mL. Each sample of 200 µL protoplast in MMG was gently mixed with less than 20uL plasmid vectors
665 (quantity described below for each individual experiment) followed by 220 µL of PEG solution and kept in darkness for
666 5 min. Next, 920 µL of W5 solution was added immediately to stop transformation. The transformed sample was
667 washed once in W5 and re-suspended in 1mL W5 solution. Samples were kept under weak light (~200 lux) for 12h
668 before downstream experimentation. The composition of the solutions noted above are identical to those in Yoo et al.
669 2007.
670
671 **BiFC and quantification**
672 Protoplast samples were transformed with 3.5 µg *pM1089::ADF* and 7 µg *pH1097::WRKY*. After 12h, images containing
673 both BiFC fluorescence and chlorophyll fluorescence were collected by confocal microscopy, with low magnification
674 (10X) and maximum pinhole (~600 nm) to include large quantities of entire cells. To obtain the most accurate and
675 comparable results, the laser and sensor settings were optimized to avoid saturation and maximize the color depth,
676 which is fixed for the total experiment. Cut-off thresholds defining system ground noise in BiFC and chlorophyll channel
677 respectively are manually determined by mock sample (i.e., pM1089::ADF4 or *pH1097::WRKY29* only). The pixel
678 brightness of BiFC and chlorophyll channels in sample images were globally subtracted by the thresholds and the
679 minus pixels were re-valued to 0. Finally, pixel brightnesses of both channels were summed; BiFC intensity was defined
680 by BiFC signal per chlorophyll signal (reflecting live cells).
681
682 **Promoter reporter assay**
683 Protoplast samples were transformed with 6 µg *pBGWϕ::pW29/pBAG7/pW46/pW48* (*eGFP* driven by WRKY induced
684 promoter), together w/o 3 µg *p5GWR::WRKY* (WRKY-mCherry) and/or 7µg *p5GWB::ADF* (ADF4-mTagBFP). Images were
685 captured using the same approach as described above for BiFC, with four channels – mTagBFP, eGFP, mCherry, and
686 chlorophyll. Similar to semi-quantitative BiFC, GFP/chlorophyll (above background threshold) was calculated for the
687 general comparison of ADF-WRKY regulated promoter intensity. Other channels were used to inspect whether
688 considerable differences of ADF and WRKY quantities may influence the system.

ChIP-qPCR

For chromatin immunoprecipitation (ChIP) qPCR, 600 µL of protoplast in MMG solution (appx. 2×10^5 protoplasts) were transformed with 15 µg *p5GWM::WRKY*, with and without 30µg *p5GWH::ADF*. For flg22 treatment, flg22 was used at a final concentration of 1 µM, and was added to the sample 1h before harvesting. After a 12h incubation period, the samples were crosslinked, purified, sonicated, homogenized for IP, using Pierce™ Classic Magnetic IP/Co-IP Kit (Thermo # 88804) following the manufacturer's instructions. Sonication was performed using a Branson CPX5800 ultrasonicator for a total of 30 min. After overnight immunoprecipitation (IP), followed by removal of the DNA crosslinking, the pulled-down DNA fraction, as well as input samples, were collected using the Zymoclean Gel DNA Recovery Kit (Zymo Research, #4008). Elution buffer (45 µL; not containing EDTA) was used to dissolve the DNA sample for ChIP-qPCR. For each run, 2 µL of eluted DNA was used as template with 3 technical repeats. Related primers are listed in Supplemental Material 5.

ChIP-seq

For ChIP sequencing (ChIP-seq), the same method used for ChIP-qPCR was followed, yet each 600 µL of protoplast sample was eluted with only 20 µL of elution buffer. The distribution of fragmented DNA size was inspected using a TapeStation system (Agilent 4200) to ensure that the majority of the DNA was between 200-400bp. The library was prepared using the Takara ThruPLEX DNA-Seq Kit (Takara, #R400674) and inspected using the TapeStation. The sequencing was performed using 75 bp paired end mode on an Illumina NEXTSEQ 500.

The analysis of the sequencing output was evaluated for quality control, and sequencing adapters were removed from the reads. Burrows-Wheeler Aligner (BWA) was used to align the reads; results with size >900bp, or quality score < 20, or non-nuclear fragments were eliminated from further analysis. Three biological repeats were pooled together. The peak-calling of the filtered alignments is conducted by MACS3 (Zhang et al. 2008) with default setting, with band width set to 250 and without sub-peaking. ChIP input is used as the control dataset. Single peaks are filtered by such criteria as: (1) they are aligned to promoter regions, (2) both p-value and q-value > 20, and (3) enrichment fold (*EF*) > 2. We define *Total Enrichment Fold* (*TEF*) to evaluate the level of ChIP enrichment on promoters since a promoter may have multiple peaks, as $TEF = 2^{\sqrt{\sum(log_2 EF)^2}}$. By default, promoters with *TEF* > 3 for A4H group (see Fig. 5A), and *TEF* > 6 for others were defined as enriched promoters, unless otherwise specified. For differential peak analysis and cis-element enrichment analysis, an independent peak-calling was conducted using the same setting, except for enabling sub-peaking to increase resolution. Differential peak analysis was conducted using the MACS3 bdgdiff function. Cis-element enrichment analysis was conducted by MEME-ChIP (Bailey et al. 2015) using the ±250bp of the summit base of each peak, and resulted consensus motifs was profiled using footprintDB (Sebastian and Contreras-Moreira 2014).

mRNA-seq

Plant RNA was extracted using the RNeasy Plant Mini kit (Qiagen # 74904) following the manufacturer's instructions. Libraries were prepared using the Roche KAPA HyperPrep RNA Library Preparation Kit with KAPA Unique Dual Index (UDI) adapters following manufacturer's recommendations. Synthesized libraries passing standard quality control were quantified using a combination of Qubit dsDNA HS and Agilent 4200 TapeStation HS DNA1000 assays. The libraries were pooled in equimolar amounts and quantified using the Invitrogen Collibri Quantification qPCR kit. The pool was loaded onto a single lane of a NovaSeq S4 flow cell, and sequencing was performed in a 2x150bp paired-end format using a NovaSeq 6000 v1.5 300 cycle reagent kit. Base calling was performed using Illumina Real Time Analysis (RTA) v3.4.4. Output of RTA was demultiplexed and converted to FastQ format with Illumina Bcl2fastq v2.20.0.

Data pre-processing, including quality control, adapter trimming, quality filtering, is conducted using FASTP (Chen et al. 2018), with default setting. Reads are counted using Salmon (Patro et al. 2017), with default setting plus --allowDovetail and --recoverOrphans. DEGs are called using DEseq2 (Love et al. 2014), and GO enrichment analysis is conducted through clusterProfiler (Wu et al. 2021). DEseq2 and clusterProfiler are performed in R environments, and others in Python. Additional descriptions are provided in figure legends.

Transcriptional profile analysis of ACTs, ADFs, and WRKYs

Arabidopsis mRNA-seq dataset GSE85932 and GSE151885 were downloaded and decompressed. Raw data was trimmed by Trimmomatic using the default settings to eliminate barcode and low-quality reads. Reads were quantified by Salmon using the same setting as described in mRNA-seq method above. For GSE151885 dataset only, the absolute quantification of all groups was deduced from the 0h group absolute quantification and the relative quantification compared to the 0h group.

Data availability

TurboID (Supplemental Material 1), ChIP-seq (Supplemental Material 2), and mRNA-seq (Supplemental Material 3) counting data will be provided as supplemental material upon formal acceptance of the peer-reviewed article. Raw data of ChIP-seq and mRNA-seq will also be made available at the same time.

Acknowledgements

We would like to appreciate Dr. Li Zhang (Soochow University, previously Michigan State University, MSU) for providing technical guidance over CRISPR knocking-out approaches. We would like to appreciate Dr. Noriko Inada (Osaka Metropolitan University) generously sharing corresponding plant materials. We would like to appreciate Dr. Steven Chou (UConn Health, University of Connecticut) for tremendous, unspoken intellectual input related to protein-protein interaction methods. We would like to appreciate Dr. Christopher Contag (MSU) and Dr. Michael H. Bachmann (MSU) for unspoken material and intellectual support for extensive studies in mammalian expression systems. We would like to appreciate Dr. Bruce L. Goode (Brandeis University) for significant intellectual input related to *Hs*DAH. We would like to appreciate Dr. Huan Chen for technical suggestions for bioinformatics. We would like to appreciate Jiahui Gong (MSU) for technical guidance over *P. carotovorum* growth assay.

Research in MSU was supported by grants from the National Science Foundation (MCB-1953014) and the National Institutes of General Medical Sciences (1R01GM125743). Research in UMD-IBBR was supported by National Science Foundation (IOS-2224203).

Conflict interest

The authors affirm that there are no conflict interests of concern.

Reference

Bailey TL, Johnson J, Grant CE, and Noble WS. The MEME Suite. Nucleic Acids Research. 2015:**43**(W1):W39–W49. https://doi.org/10.1093/nar/gkv416

Birkenbihl RP, Kracher B, Roccaro M, and Somssich IE. Induced Genome-Wide Binding of Three Arabidopsis WRKY Transcription Factors during Early MAMP-Triggered Immunity. The Plant Cell. 2017:**29**(1):20–38. https://doi.org/10.1105/tpc.16.00681

Branon TC, Bosch JA, Sanchez AD, Udeshi ND, Svinkina T, Carr SA, Feldman JL, Perrimon N, and Ting AY. Efficient proximity labeling in living cells and organisms with TurboID. Nat Biotechnol. 2018:**36**(9):880–887. https://doi.org/10.1038/nbt.4201

Chen H and Day B. Insights into Immune Gene Prediction and Function Through the Evolutionary History of ADF Gene Family. 2024:2024.05.31.596878. https://doi.org/10.1101/2024.05.31.596878

Chen S, Zhou Y, Chen Y, and Gu J. fastp: an ultra-fast all-in-one FASTQ preprocessor. Bioinformatics. 2018:**34**(17):i884–i890. https://doi.org/10.1093/bioinformatics/bty560

Dong C-H and Hong Y. Arabidopsis CDPK6 phosphorylates ADF1 at N-terminal serine 6 predominantly. Plant Cell Rep. 2013:**32**(11):1715–1728. https://doi.org/10.1007/s00299-013-1482-6

786 **Dopie J, Skarp K-P, Kaisa Rajakylä E, Tanhuanpää K, and Vartiainen MK**. Active maintenance of nuclear actin by
787 importin 9 supports transcription. Proceedings of the National Academy of Sciences. 2012:**109**(9):E544–
788 E552. https://doi.org/10.1073/pnas.1118880109

789 **Du J, Wang X, Dong C-H, Yang JM, and Yao XJ**. Computational Study of the Binding Mechanism of Actin-
790 Depolymerizing Factor 1 with Actin in Arabidopsis thaliana. PLOS ONE. 2016:**11**(7):e0159053.
791 https://doi.org/10.1371/journal.pone.0159053

792 **García-González J and van Gelderen K**. Bundling up the Role of the Actin Cytoskeleton in Primary Root Growth.
793 Front Plant Sci. 2021:**12**. https://doi.org/10.3389/fpls.2021.777119

794 **Inada N, Higaki T, and Hasezawa S**. Nuclear Function of Subclass I Actin-Depolymerizing Factor Contributes to
795 Susceptibility in Arabidopsis to an Adapted Powdery Mildew Fungus. Plant Physiology. 2016:**170**(3):1420–
796 1434. https://doi.org/10.1104/pp.15.01265

797 **Javed T and Gao S-J**. WRKY transcription factors in plant defense. Trends in Genetics. 2023:**39**(10):787–801.
798 https://doi.org/10.1016/j.tig.2023.07.001

799 **Jones JDG, Staskawicz BJ, and Dangl JL**. The plant immune system: From discovery to deployment. Cell.
800 2024:**187**(9):2095–2116. https://doi.org/10.1016/j.cell.2024.03.045

801 **Kloc M, Chanana P, Vaughn N, Uosef A, Kubiak JZ, and Ghobrial RM**. New Insights into Cellular Functions of
802 Nuclear Actin. Biology. 2021:**10**(4):304. https://doi.org/10.3390/biology10040304

803 **Kyheröinen S and Vartiainen MK**. Nuclear actin dynamics in gene expression and genome organization. Seminars in
804 Cell & Developmental Biology. 2020:**102**:105–112. https://doi.org/10.1016/j.semcdb.2019.10.012

805 **Lappalainen P, Kotila T, Jégou A, and Romet-Lemonne G**. Biochemical and mechanical regulation of actin
806 dynamics. Nat Rev Mol Cell Biol. 2022:**23**(12):836–852. https://doi.org/10.1038/s41580-022-00508-4

807 **Li P and Day B**. Battlefield Cytoskeleton: Turning the Tide on Plant Immunity. MPMI. 2019:**32**(1):25–34.
808 https://doi.org/10.1094/MPMI-07-18-0195-FI

809 **Li P, Zhang Z, Tong Y, Foda BM, and Day B**. ILEE: Algorithms and toolbox for unguided and accurate quantitative
810 analysis of cytoskeletal images. Journal of Cell Biology. 2022:**222**(2):e202203024.
811 https://doi.org/10.1083/jcb.202203024

812 **Li W, Pang S, Lu Z, and Jin B**. Function and Mechanism of WRKY Transcription Factors in Abiotic Stress Responses of
813 Plants. Plants. 2020:**9**(11):1515. https://doi.org/10.3390/plants9111515

814 **Love MI, Huber W, and Anders S**. Moderated estimation of fold change and dispersion for RNA-seq data with
815 DESeq2. Genome Biol. 2014:**15**(12):550. https://doi.org/10.1186/s13059-014-0550-8

816 **Lu Y, Zhang Y, Lian N, and Li X**. Membrane Dynamics Regulated by Cytoskeleton in Plant Immunity. International
817 Journal of Molecular Sciences. 2023:**24**(7):6059. https://doi.org/10.3390/ijms24076059

818 **Lu Y-J, Li P, Shimono M, Corrion A, Higaki T, He SY, and Day B**. Arabidopsis calcium-dependent protein kinase 3
819 regulates actin cytoskeleton organization and immunity. Nat Commun. 2020:**11**(1):6234.
820 https://doi.org/10.1038/s41467-020-20007-4

821 **Mair A, Xu S-L, Branon TC, Ting AY, and Bergmann DC**. Proximity labeling of protein complexes and cell-type-
822 specific organellar proteomes in Arabidopsis enabled by TurboID. eLife. 2019:**8**:e47864.
823 https://doi.org/10.7554/eLife.47864

824 **Mao Y, Zhang H, Xu N, Zhang B, Gou F, and Zhu J-K**. Application of the CRISPR–Cas System for Efficient Genome
825 Engineering in Plants. Molecular Plant. 2013:**6**(6):2008–2011. https://doi.org/10.1093/mp/sst121

826 **Matsumoto T, Higaki T, Takatsuka H, Kutsuna N, Ogata Y, Hasezawa S, Umeda M, and Inada N**. Arabidopsis
827 thaliana Subclass I ACTIN DEPOLYMERIZING FACTORs Regulate Nuclear Organization and Gene Expression.
828 Plant and Cell Physiology. 2023:**64**(10):1231–1242. https://doi.org/10.1093/pcp/pcad092

829 **Matsumoto T, Kobayashi K, and Inada N**. Arabidopsis thaliana ACTIN DEPOLYMERIZING FACTORs play a role in leaf
830 senescence regulation. 2024:2024.05.14.594232. https://doi.org/10.1101/2024.05.14.594232

831 **McDowell JM, Huang S, McKinney EC, An Y-Q, and Meagher RB**. Structure and Evolution of the Actin Gene Family in
832 Arabidopsis thaliana. Genetics. 1996:**142**(2):587–602. https://doi.org/10.1093/genetics/142.2.587

833 **Patro R, Duggal G, Love MI, Irizarry RA, and Kingsford C**. Salmon provides fast and bias-aware quantification of
834 transcript expression. Nat Methods. 2017:**14**(4):417–419. https://doi.org/10.1038/nmeth.4197

835 **Pollard TD and Goldman RD**. Overview of the Cytoskeleton from an Evolutionary Perspective. Cold Spring Harb
836 Perspect Biol. 2018:**10**(7):a030288. https://doi.org/10.1101/cshperspect.a030288

837 **Porter K, Shimono M, Tian M, and Day B**. Arabidopsis Actin-Depolymerizing Factor-4 Links Pathogen Perception,
838 Defense Activation and Transcription to Cytoskeletal Dynamics. PLOS Pathogens. 2012:**8**(11):e1003006.
839 https://doi.org/10.1371/journal.ppat.1003006

840 **Qin L, Liu L, Tu J, Yang G, Wang S, Quilichini TD, Gao P, Wang H, Peng G, Blancaflor EB, et al.** The ARP2/3
841 complex, acting cooperatively with Class I formins, modulates penetration resistance in Arabidopsis against
842 powdery mildew invasion. The Plant Cell. 2021:**33**(9):3151–3175. https://doi.org/10.1093/plcell/koab170

843 **Saile SC, Jacob P, Castel B, Jubic LM, Salas-Gonzáles I, Bäcker M, Jones JDG, Dangl JL, and Kasmi FE**. Two
844 unequally redundant "helper" immune receptor families mediate Arabidopsis thaliana intracellular "sensor"
845 immune receptor functions. PLOS Biology. 2020:**18**(9):e3000783.
846 https://doi.org/10.1371/journal.pbio.3000783

847 **Sebastian A and Contreras-Moreira B**. footprintDB: a database of transcription factors with annotated cis elements
848 and binding interfaces. Bioinformatics. 2014:**30**(2):258–265. https://doi.org/10.1093/bioinformatics/btt663

849 **Sharma A and Chandran D**. Host nuclear repositioning and actin polarization towards the site of penetration
850 precedes fungal ingress during compatible pea-powdery mildew interactions. Planta. 2022:**256**(2):45.
851 https://doi.org/10.1007/s00425-022-03959-3

852 **Shehjar F, Almarghalani DA, Mahajan R, Hasan SA-M, and Shah ZA**. The Multifaceted Role of Cofilin in
853 Neurodegeneration and Stroke: Insights into Pathogenesis and Targeting as a Therapy. Cells. 2024:**13**(2):188.
854 https://doi.org/10.3390/cells13020188

855 **Sinha J, Singh Y, and Verma PK**. Cytoskeleton remodeling: a central player in plant–fungus interactions. Journal of
856 Experimental Botany. 2024:**75**(11):3269–3286. https://doi.org/10.1093/jxb/erae133

857 **Sun Y, Shi M, Wang D, Gong Y, Sha Q, Lv P, Yang J, Chu P, and Guo S**. Research progress on the roles of actin-
858 depolymerizing factor in plant stress responses. Front Plant Sci. 2023:**14**.
859 https://doi.org/10.3389/fpls.2023.1278311

860 **Tanaka K, Takeda S, Mitsuoka K, Oda T, Kimura-Sakiyama C, Maéda Y, and Narita A**. Structural basis for cofilin
861 binding and actin filament disassembly. Nat Commun. 2018:**9**(1):1860. https://doi.org/10.1038/s41467-018-
862 04290-w

Teliska LH and Rasband MN. Spectrins. Current Biology. 2021:**31**(10):R504–R506. https://doi.org/10.1016/j.cub.2021.01.040

Tian F, Yang D-C, Meng Y-Q, Jin J, and Gao G. PlantRegMap: charting functional regulatory maps in plants. Nucleic Acids Research. 2020:**48**(D1):D1104–D1113. https://doi.org/10.1093/nar/gkz1020

Tian M, Chaudhry F, Ruzicka DR, Meagher RB, Staiger CJ, and Day B. Arabidopsis Actin-Depolymerizing Factor AtADF4 Mediates Defense Signal Transduction Triggered by the Pseudomonas syringae Effector AvrPphB. Plant Physiology. 2009:**150**(2):815–824. https://doi.org/10.1104/pp.109.137604

Van Ngo H and Mostowy S. Role of septins in microbial infection. Journal of Cell Science. 2019:**132**(9). https://doi.org/10.1242/jcs.226266

Wang J, Lian N, Zhang Y, Man Y, Chen L, Yang H, Lin J, and Jing Y. The Cytoskeleton in Plant Immunity: Dynamics, Regulation, and Function. International Journal of Molecular Sciences. 2022:**23**(24):15553. https://doi.org/10.3390/ijms232415553

Wei M, Fan X, Ding M, Li R, Shao S, Hou Y, Meng S, Tang F, Li C, and Sun Y. Nuclear actin regulates inducible transcription by enhancing RNA polymerase II clustering. Science Advances. 2020:**6**(16):eaay6515. https://doi.org/10.1126/sciadv.aay6515

Wu F-H, Shen S-C, Lee L-Y, Lee S-H, Chan M-T, and Lin C-S. Tape-Arabidopsis Sandwich - a simpler Arabidopsis protoplast isolation method. Plant Methods. 2009:**5**(1):16. https://doi.org/10.1186/1746-4811-5-16

Wu T, Hu E, Xu S, Chen M, Guo P, Dai Z, Feng T, Zhou L, Tang W, Zhan L, et al. clusterProfiler 4.0: A universal enrichment tool for interpreting omics data. Innovation. 2021:**2**(3). https://doi.org/10.1016/j.xinn.2021.100141

Wu Y, Sexton WK, Zhang Q, Bloodgood D, Wu Y, Hooks C, Coker F, Vasquez A, Wei C-I, and Xiao S. Leaf abaxial immunity to powdery mildew in Arabidopsis is conferred by multiple defense mechanisms. Journal of Experimental Botany. 2024:**75**(5):1465–1478. https://doi.org/10.1093/jxb/erad450

Xing J, Wang Y, Peng A, Li J, Niu X, and Zhang K. The role of actin cytoskeleton CFL1 and ADF/cofilin superfamily in inflammatory response. Front Mol Biosci. 2024:**11**. https://doi.org/10.3389/fmolb.2024.1408287

Yao N, Li J, Liu H, Wan J, Liu W, and Zhang M. The Structure of the ZMYND8/Drebrin Complex Suggests a Cytoplasmic Sequestering Mechanism of ZMYND8 by Drebrin. Structure. 2017:**25**(11):1657-1666.e3. https://doi.org/10.1016/j.str.2017.08.014

Yoo S-D, Cho Y-H, and Sheen J. Arabidopsis mesophyll protoplasts: a versatile cell system for transient gene expression analysis. Nat Protoc. 2007:**2**(7):1565–1572. https://doi.org/10.1038/nprot.2007.199

Yu H, Maoliniyazi M, Han X, Yang H, Zhang Z, Guo Y, Tang X, Li H, Cao Q, Wang S, et al. YUCCA3 interacts with ADF4 to regulate *Arabidopsis* hypocotyl elongation by organizing actin arrays. Plant Physiology and Biochemistry. 2025:**223**:109877. https://doi.org/10.1016/j.plaphy.2025.109877

Yuan M, Jiang Z, Bi G, Nomura K, Liu M, Wang Y, Cai B, Zhou J-M, He SY, and Xin X-F. Pattern-recognition receptors are required for NLR-mediated plant immunity. Nature. 2021:**592**(7852):105–109. https://doi.org/10.1038/s41586-021-03316-6

Zhang Y, Liu T, Meyer CA, Eeckhoute J, Johnson DS, Bernstein BE, Nusbaum C, Myers RM, Brown M, Li W, et al. Model-based Analysis of ChIP-Seq (MACS). Genome Biology. 2008:**9**(9):R137. https://doi.org/10.1186/gb-2008-9-9-r137

902 **Zhao S, Jiang Y, Zhao Y, Huang S, Yuan M, Zhao Y, and Guo Y**. CASEIN KINASE1-LIKE PROTEIN2 Regulates Actin
903 Filament Stability and Stomatal Closure via Phosphorylation of Actin Depolymerizing Factor. The Plant Cell.
904 2016:**28**(6):1422–1439. https://doi.org/10.1105/tpc.16.00078

905

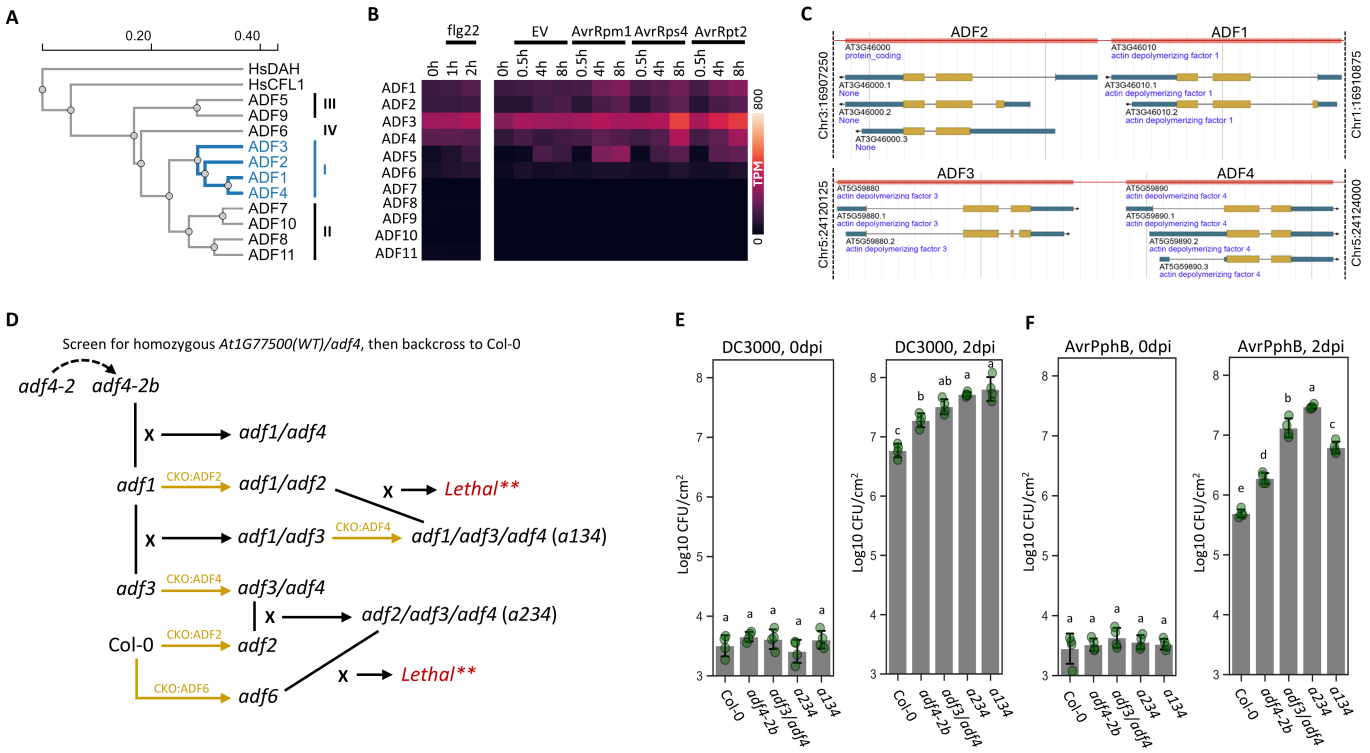

Figure 1: Class I ADF redundantly contributes to Resistance against Pseudomonas syringae. A, Phylogenic tree of Arabidopsis ADFs based on proteins sequence. Class I-IV are illustrated. Human CFL1 and Drebrin ADF-H domain (DAH) are also included, which are shown distinct from Arabidopsis ADFs. B, temporal expression profile of Arabidopsis ADFs in PTI and ETI. Public mRNA-seq datasets GSE85932 (PTI) and GSE151885 (ETI) are downloaded and analyzed. Expression levels are represented by TPM. C, genome map of ADF1/2/3/4. ADF1/2 and ADF3/4 are adjacent genes, which does not support the generation of their high order mutants by crossing. D, technical routine to construct ADF high order mutants combining CRISPR and crossing. **, presumably lethal because no homozygous progenies are identified through multiple attempts. E-F, *P. syringae* growth assay using ADF high order mutants. DC3000 (E) or DC3000/AvrPphB (F) at OD600 = 0.002 are infiltrated to 5-week-old Arabidopsis. Infected leaf samples are measured at 2dpi. ADF high order mutants significantly enhance susceptibility to DC3000 and AvrPphB. Data pass ANOVA with $P<0.05$; for multiple comparison, non-overlapping alphabets suggest $P<0.05$ upon post-hoc T-tests adjusted by Benjamini–Hochberg procedure for family-wise error.

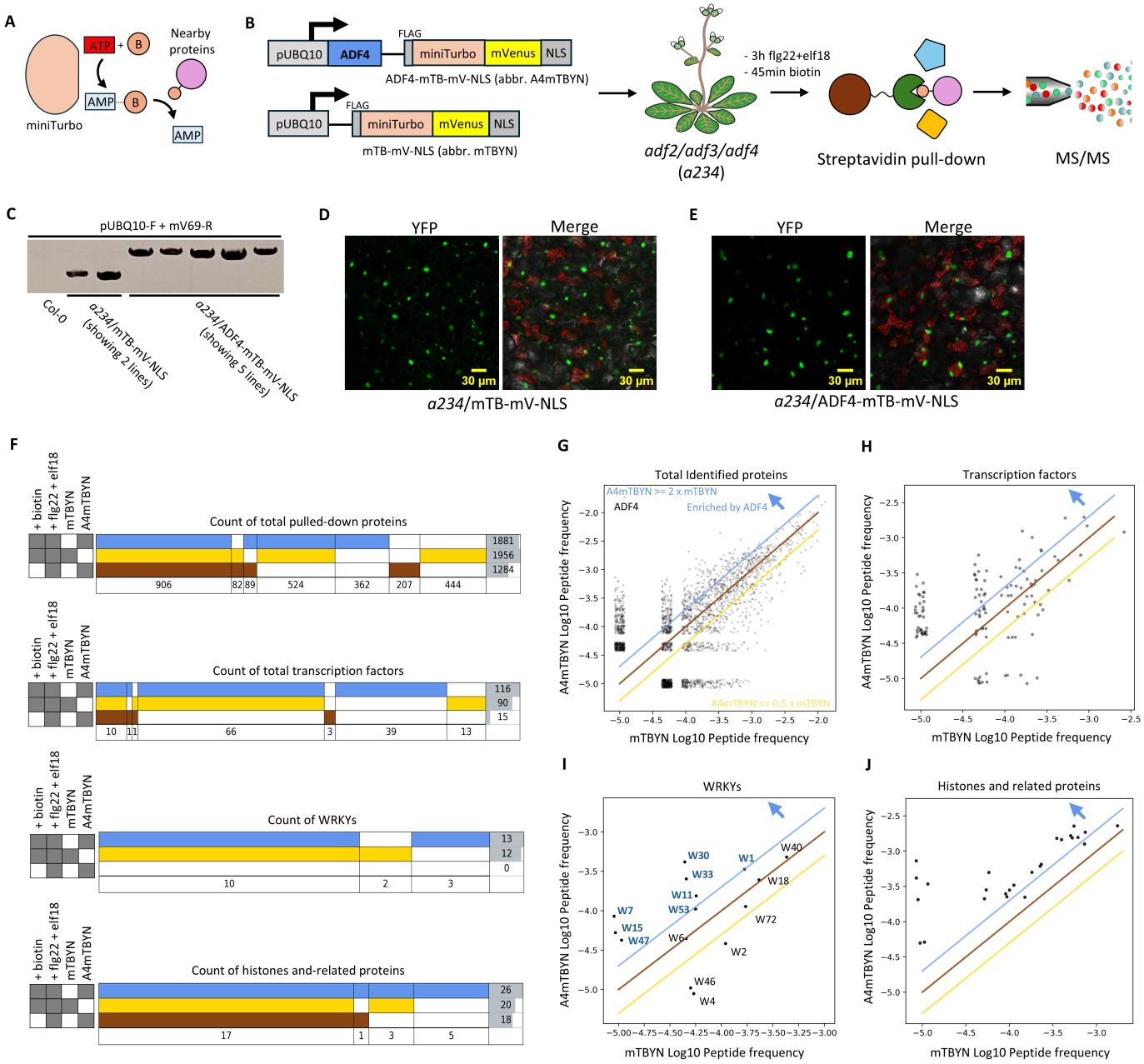

Figure 2: Identification of ADF4 interactors in nucleus using TurboID. A, TurboID mechanism. miniTurbo-fused interested protein transfers its nearby interacted protein with a covalent biotin tag (shown as "B"), to be used for interactome enrichment. B. Experiment scheme. ADF4 are fused by miniTurbo-mVenus-NLS (mTBYN) using a flexible linker, driven by pUBQ10. This ORF is transformed into *a234* background. Plants are treated with PAMPs to induce pro-immune proteome, followed by biotin to activate labelling. ADF4-interactive in the nucleus are IP-ed and identified through MS/MS. Plants with miniTurbo-mVenus-NLS construct without ADF4 is used as the negative control. C, genotypic identification of turboID constructs. D-E, subcellular localization of mTBYN (D) and ADF4-mTBYN (A4mTBYN; E) in Arabidopsis. Both exhibit exclusive nuclear localization. F, SuperVenn diagrams of ADF4-specific and non-specific TurboID-labelled interactome, in the order of total pulldown, transcription factors, WRKYs, and histone related proteins, from top to bottom. Note that SuperVenn is modified format of Venn diagram with flattened layout, with unlimited upper

934 limit of set number. G-J, quantitative distribution of ADF4-enriched proteins. Scatter plots are used to show the
935 relationship of logarithmic peptide frequency in mTBYN vs A4mTBYN of identified proteins, in terms of total protein (G),
936 TFs (H), WRKYs (I), and Histone related proteins (J). Frequency of "0" is re-valued to 1e-5 to enable visualization. A point
937 jitter is applied to visualize overlapping points. Blue line, A4mTBYN = 2 * mTBYN; brown line, A4mTBYN = mTBYN; yellow
938 line, A4mTBYN = 0.5 * mTBYN. The distance from a top-left point to the brown line represents the protein's enrichment
939 level by ADF4. We define the proteins at the top-left of the blue line as the potential ADF4 interactive proteins.

A

Basic information of selected WRKY candidates

Gene	Group*	Phenotype by pathogen:	Upreg. by immunity	Identified by TurboID
WRKY4	Ia	P.s. (B), Bo.c.,	No	Yes
WRKY33		Bo.c.	Yes	Yes, ADF4-enriched
WRKY8	Ib	P.s. (B, ETI), TMV	Yes	No
WRKY28		P.s. (ETI), Bo.c.	Yes	No
WRKY48		P.s. (B, ETI)	Yes	No
WRKY18	IIa	P.s. (B), G.o.	Yes	Yes
WRKY40		G.o.	Yes	Yes
WRKY6	IIb	-	Yes	Yes
WRKY11	IIc	P.s. (B), Ba.c. (ISR)	Yes	Yes, ADF4-enriched
WRKY17			Yes	No
WRKY22	IId	P.s. (B, PTI)	Yes	No
WRKY29		General PTI marker	Yes	No
WRKY30	IIIa	CMV	Yes	Yes, ADF4-enriched
WRKY46		P.s. (B)	Yes	Yes
WRKY70		P.s. (B), *H.p.*	Yes	No
WRKY38	IIIb	P.s. (B)	No	No

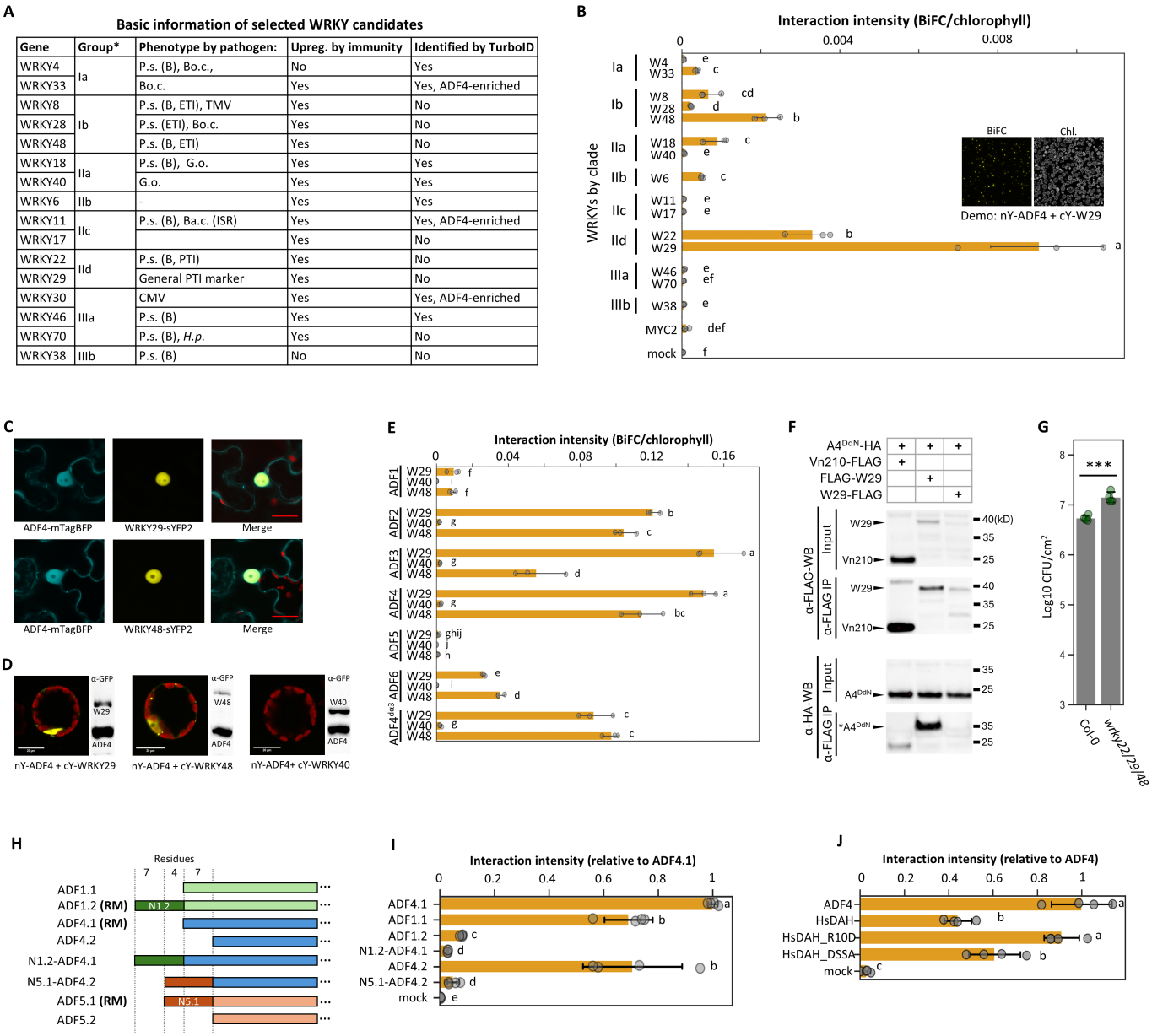

Figure 3: ADFs and WRKYs specifically interact with each other. A, information of selected WRKY candidates. Arabidopsis WRKYs are selected to test their capability to interact with ADFs, based on their phylogenic group, immune phenotypes, induction profile, and TurboID identification. B, ADF4-interaction affinity of selected WRKYs by Semi-quantitative BiFC. Controlled amount of nY-ADF4 and cY-WRKYs are transformed into Col-0 protoplast. After 12h, large scale confocal images, shown as demo, are taken for computational analysis. BiFC/chlorophyll is used to evaluate interaction intensity. WRKY22/29/48 show strong interaction with ADF4. C, subcellular localization of ADF4 and WRKY29 in *N. benthiamiana*. D, single cell image of ADF4-WRKYs BiFC. Most interaction occurs in the nucleus with minor signal in vesicle-like structures. Respective immunoblots are conducted to confirm similar amount of ADF and WRKYs are produced for the experiment system. E, Arabidopsis ADFs have varied interaction intensity to WRKYs. For BiFC, controlled amount of nY-ADFs are co-transformed with cY-WRKY29/48 or cY-WRKY40 as a negative control. ADF2/3/4 show strong interaction with WRKY29/48. Actin-non-interactive ADF4 mutant, ADF4^{dα3}, still maintains WRKY interaction activity. F, CoIP demonstrating ADF4-WRKY29 interaction. ADF4$^{S6D/dα3}$-NLS (abbr. A4^{DdN}) was used as an

954 alternative of wild type ADF4, to eliminate actin binding competition and improve WRKY affinity. mVenus1-210 (abbr.
955 Vn210), the n-terminal nuclear permeable fraction of mVenus usually used for BiFC, was used as a negative control.
956 FLAG-WRKY29 enriched an unknown modified version of $A4^{DdN}$-HA (marked as "*"), but WRKY29-FLAG cannot mediate
957 any interaction. Extremely strong expression of Vn210 introduced a minor non-specific interaction with $A4^{DdN}$. G, *P.*
958 *syringae* DC3000 growth assay on triple mutant *wrky22/29/48*. *wrky22/29/48* has dampened resistance, phenocopying
959 *a234* (Fig. 1E). H, Alternative splicing of ADF1/4/5 on the N-terminus and design of their chimera. ADF1/4/5 alternative
960 splicing models are aligned according to protein sequence homogeneity. The first 11 AA of ADF1.2 are fused to ADF4.1,
961 making N1.2-ADF4.1N; the first 11 AA of ADF5.1 are fused to ADF4.2 to make N5.1-ADF4.2. RM, TAIR representative
962 gene model. I, N-terminal sequence of ADFs significantly impact ADF-WRKY interaction. Different transcription models
963 and their chimeras of ADF are co-transformed with cY-WRKY29 for BiFC. N1.2 inhibits the interaction of ADF1.1/4.1
964 and WRKKY29; N5.1 inhibits the interaction of ADF4.2. J, human drebrin ADF domain (HsDAH) interacts with WRKY29
965 using an interface different from HsDAH-ZMYND8 interaction. HsDAH, and its single mutant R10D and quadruple
966 mutant R10D/L14S/C96S/E107A (DSSA), on critical residues mediating HsDAH-ZMYND8 interface, are co-transformed
967 with WRKY29 for BiFC. HsDAH interacts with WRKY29 with a minorly reduced intensity compared with ADF4, but R10D
968 or DSSA mutant do not impact the interaction. All data pass ANOVA with $P<0.05$; for multiple comparison, non-
969 overlapping alphabets suggest $P<0.05$ upon post-hoc T-tests adjusted by Benjamini–Hochberg procedure for family-
970 wise error.
971

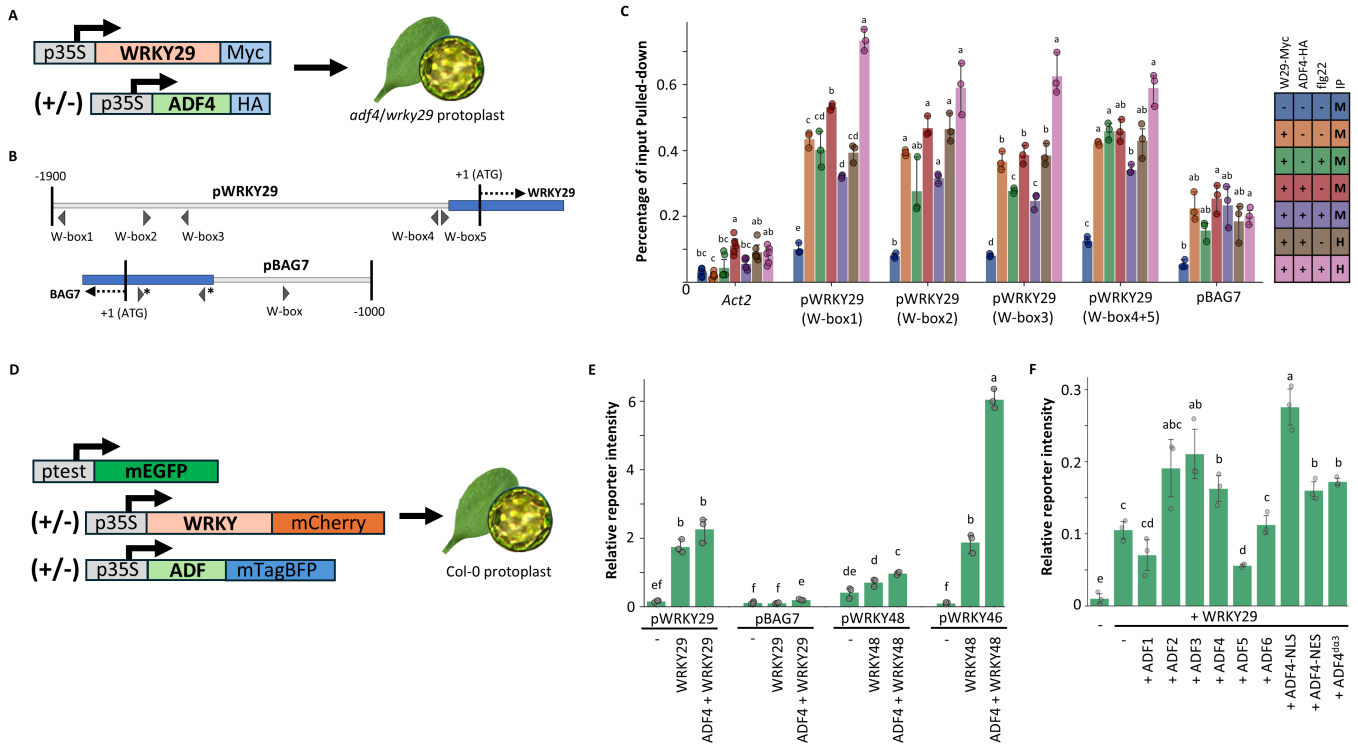

Figure 4: ADFs associates with WRKYs at targeted promoters and regulate gene expression level. A, experiment scheme of ADF4-WRKY29 ChIP assay. B, distribution of W-boxes on pWRKY29 and pBAG7. C, ChIP-qPCR quantification of W-box fragments enriched by WRKY29 and ADF4. WRKY29 and ADF4 (when co-expressed with WRKY29) can enrich pWRKY29 and pBAG7 fragments. Act2 gene serves as the negative control of targeted DNA. flg22 does not significantly influence the binding affinity of WRKY29 and ADF4. D, experiment scheme of promoter reporter assay. E, promoter reporter assay of WRKY29/48 on different promoters. F, promoter reporter assay testing the impact of different ADFs on WRKY29-targeted pWRKY29. All data pass ANOVA with $P<0.05$; for multiple comparison, non-overlapping alphabets suggest $P<0.05$ upon post-hoc T-tests adjusted by Benjamini–Hochberg procedure for family-wise error.

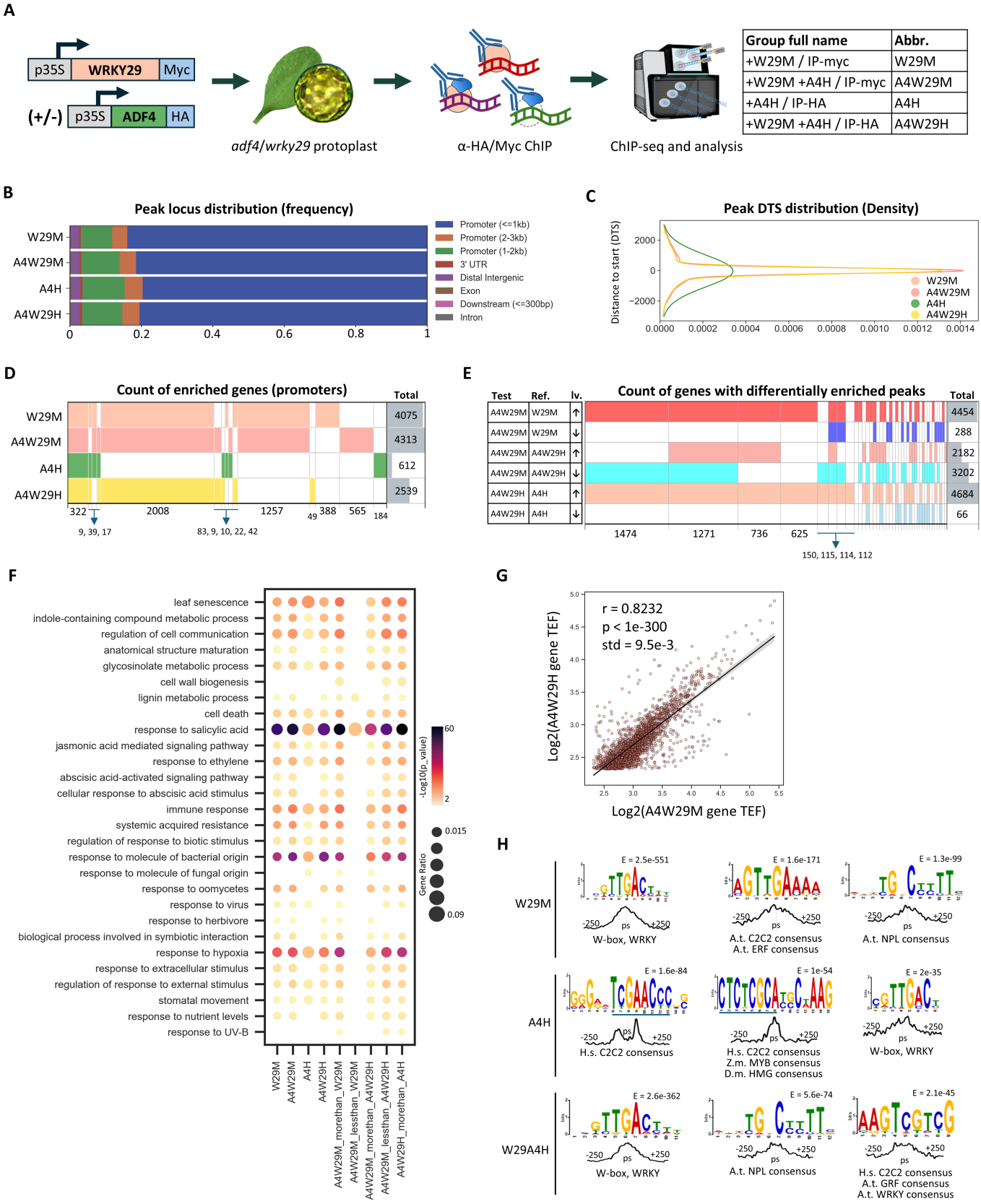
A
p35S
WRKY29
Myc
(+/-)
p35S
ADF4
HA
adf4/wrky29 protoplast
α-HA/Myc ChIP
ChIP-seq and analysis
Group full name | Abbr.
+W29M / IP-myc | W29M
+W29M +A4H / IP-myc | A4W29M
+A4H / IP-HA | A4H
+W29M +A4H / IP-HA | A4W29H
B
Peak locus distribution (frequency)
W29M
A4W29M
A4H
A4W29H
Promoter (<=1kb)
Promoter (2-3kb)
Promoter (1-2kb)
3' UTR
Distal Intergenic
Exon
Downstream (<=300bp)
Intron
C
Peak DTS distribution (Density)
Distance to start (DTS)
D
Count of enriched genes (promoters)
Total
4075
4313
612
2539
E
Count of genes with differentially enriched peaks
Test
Ref.
lv.
Total
4454
288
2182
3202
4684
66
F
leaf senescence
indole-containing compound metabolic process
regulation of cell communication
anatomical structure maturation
glycosinolate metabolic process
cell wall biogenesis
lignin metabolic process
cell death
response to salicylic acid
jasmonic acid mediated signaling pathway
response to ethylene
abscisic acid-activated signaling pathway
cellular response to abscisic acid stimulus
immune response
systemic acquired resistance
regulation of response to biotic stimulus
response to molecule of bacterial origin
response to molecule of fungal origin
response to oomycetes
response to virus
response to herbivore
biological process involved in symbiotic interaction
response to hypoxia
response to extracellular stimulus
regulation of response to external stimulus
stomatal movement
response to nutrient levels
response to UV-B
-Log10(p_value)
Gene Ratio
W29M
A4W29M
A4H
A4W29H
A4W29M_morethan_W29M
A4W29M_lessthan_W29M
A4W29M_morethan_A4W29H
A4W29M_lessthan_A4W29H
A4W29H_morethan_A4H
G
r = 0.8232
p < 1e-300
std = 9.5e-3
Log2(A4W29H gene TEF)
Log2(A4W29M gene TEF)
H
W29M
A4H
W29A4H
W-box, WRKY
A.t. C2C2 consensus
A.t. ERF consensus
A.t. NPL consensus
H.s. C2C2 consensus
Z.m. MYB consensus
D.m. HMG consensus
A.t. GRF consensus
A.t. WRKY consensus

983

984 **Figure 5: ChIP-seq reveals genome-wide immune gene promoters co-targeted by WRKY29 and ADF4.** A, the ChIP-
985 seq scheme. Experiment group abbreviations are described here. B, Peak distribution of pulled-down genome
986 fragments, by genomic function. Regardless of groups, most peaks are located on gene promoters. C, The distance-to-
987 start (DTS) distribution of peaks. D, SuperVenn diagram of enriched targeted genes overlapped or specific among
988 groups. E, SuperVenn diagram of overlapped or specific genes with differentially enriched single peaks among different
989 comparisons. F, GO pathway enrichment analysis on genes with promoter enriched by ChIP and genes with
990 differentially enriched single peaks. Selected pathways are presented. G, Correlation analysis of gene enrichment level
991 by WRKY and ADF. Scatter plot represents logarithmic enrichment level (defined by TEF, see Methods) of genes
992 identified by both A4W29M and A4W29H. A strong linear correlation with r = 0.8232 is detected, suggesting WRKY29
993 and ADF4 colocalize on their genome targeting sites. H, cis-element enrichment analysis identifies motif consensuses
994 by binding sites of WRKY and TF in other families. MEME-ChIP is used analyze the ±250bp region surrounding the
995 summit of each peak in different groups. TF binding consensus of WRKY, C2C2, ERF, NPL, MYB, and HMG family are
996 identified. Blue bar highlights nucleotides when only partial of the motif is used to identify TF binding consensus.
997

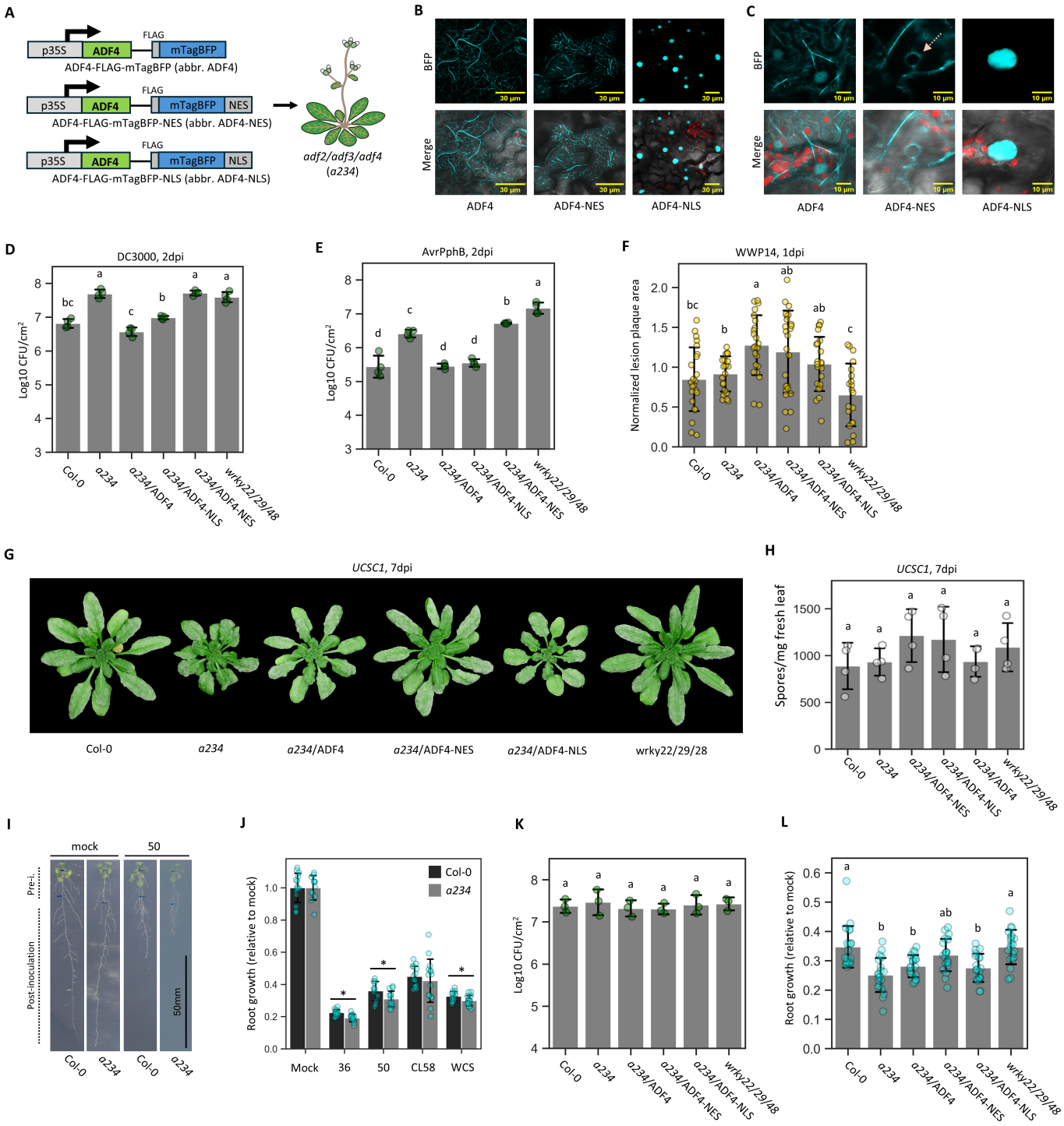

Figure 6: cytosolic and nuclear ADF4 have distinguished roles in different scenarios of plant immunity. A, Scheme of the construction of general and cytoplast/nucleus-exclusive ADF complementation lines. B-C, subcellular localization of ADF4, ADF4-NES (nuclear exiting signal), and ADF-NLS (nuclear localization signal) in Arabidopsis by low (B) and high (C) magnification. ADF4 normally localizes in both cytosol, with aggregation on actin bundle, and nucleus. NES and NLS thoroughly forced cytosolic and nuclear localization. Cyan = ADF4 (mTagBFP); red = chloroplast. Pink

dashed arrow points to an empty nucleus. D-E, *P. syringae* growth essay on different ADF complementation lines, using DC3000 (D), and DC3000/AvrPphB (E). Bacteria is inoculated to 5-week-old plants at OD600 = 0.002. Samples are harvest at 2dpi. See supplemental figure for 0dpi data. Dampened resistance in *a234* is rescued by ADF4 or majorly ADF4-NLS, but not ADF4-NES. wr*ky22/29/48* phenocopies *a234*. F, Pectinobacteria growth essay on different ADF complementation lines. Col-0, *a234*, and *w22/29/48* show no difference among each other, but overexpressing ADF4 increases susceptibility. G-H, Powdery mildew UCSC1 growth assay. No significant difference among genotypes by visual observation (G) or conidia spore quantification (H). I, demonstration picture of root commensal bacterial infection vertical plate assay (VPA). 1-week-old axenic seedlings are carefully transferred to a vertical plate previous spread with root commensal bacteria, root architectures are imaged 10 dpi to determine the developmental impact by bacteria. J, root commensal bacterial VPA on *a234*. Bacteria 36, 50, and WCS (see strain details in Methods) have enhanced growth inhibition on *a234*. K, bacteria growth in VPA on *a234* and complementation lines inoculated with 50. 50 do not show different population among Arabidopsis genotypes. L, Root growth in VPA on *a234* and the complementation lines inoculated with 50. *a234* show enhanced root growth inhibition but cannot be complemented with ADF4/ADF4-NES/NLS. *wrky22/29/48* does not phenocopies *a234*. Data of D, E, F, J, and L pass ANOVA with $P<0.05$; for multiple comparison, non-overlapping alphabets suggest $P<0.05$ upon post-hoc T-tests adjusted by Benjamini–Hochberg procedure for family-wise error.

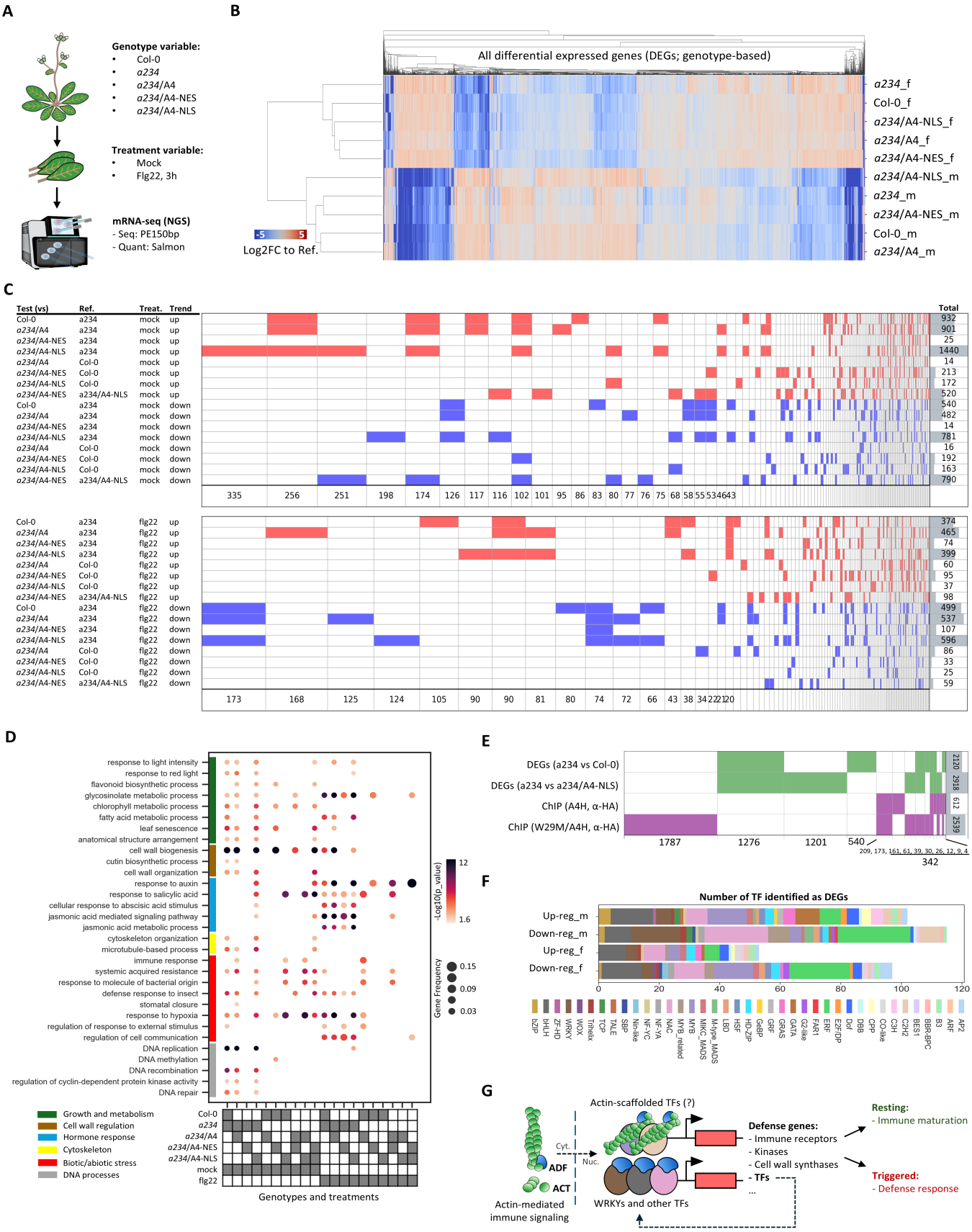
A
Genotype variable:
Col-0
a234
a234/A4
a234/A4-NES
a234/A4-NLS
Treatment variable:
Mock
Flg22, 3h
mRNA-seq (NGS)
- Seq: PE150bp
- Quant: Salmon
B
All differential expressed genes (DEGs; genotype-based)
a234_f
Col-0_f
a234/A4-NLS_f
a234/A4_f
a234/A4-NES_f
a234/A4-NLS_m
a234_m
a234/A4-NES_m
Col-0_m
a234/A4_m
-5
5
Log2FC to Ref.
C
Test (vs)
Ref.
Treat.
Trend
Total
D
response to light intensity
response to red light
flavonoid biosynthetic process
glycosinolate metabolic process
chlorophyll metabolic process
fatty acid metabolic process
leaf senescence
anatomical structure arrangement
cell wall biogenesis
cutin biosynthetic process
cell wall organization
response to auxin
response to salicylic acid
cellular response to abscisic acid stimulus
jasmonic acid mediated signaling pathway
jasmonic acid metabolic process
cytoskeleton organization
microtubule-based process
immune response
systemic acquired resistance
response to molecule of bacterial origin
defense response to insect
stomatal closure
response to hypoxia
regulation of response to external stimulus
regulation of cell communication
DNA replication
DNA methylation
DNA recombination
regulation of cyclin-dependent protein kinase activity
DNA repair
-Log10(p_value)
12
1.6
Gene Frequency
0.15
0.09
0.03
Growth and metabolism
Cell wall regulation
Hormone response
Cytoskeleton
Biotic/abiotic stress
DNA processes
Col-0
a234
a234/A4
a234/A4-NES
a234/A4-NLS
mock
flg22
Genotypes and treatments
E
DEGs (a234 vs Col-0)
DEGs (a234 vs a234/A4-NLS)
ChIP (A4H, α-HA)
ChIP (W29M/A4H, α-HA)
1787
1276
1201
540
342
F
Number of TF identified as DEGs
Up-reg_m
Down-reg_m
Up-reg_f
Down-reg_f
0
20
40
60
80
100
120
bZIP
bHLH
ZF-HD
WRKY
WOX
Trihelix
TCP
TALE
SBP
Nin-like
NF-YC
NF-YA
NAC
MYB_related
MYB
MIKC_MADS
M-type_MADS
LBD
HSF
HD-ZIP
GeBP
GRF
GRAS
GATA
G2-like
FAR1
ERF
E2Ffdp
Dof
DBB
CPP
CO-like
C3H
C2H2
BES1
BBR-BPC
B3
ARF
AP2
G
Actin-scaffolded TFs (?)
Cyt.
Nuc.
ADF
ACT
Actin-mediated immune signaling
WRKYs and other TFs
Defense genes:
- Immune receptors
- Kinases
- Cell wall synthases
- TFs
...
Resting:
- Immune maturation
Triggered:
- Defense response

1023 **Figure 7: Nuclear ADF4 mediates transcriptomic regulation at resting state and PTI event.** A, mRNA-seq
1024 experiment scheme. B, DEG clustering analysis. Heatmap represents logrithmic fold-of-change of TPM compared to
1025 a234 of all DEGs, which is clustered by their cross-group patterns. DEG is identified by DEseq2, defined by significant
1026 deference of FPKM across any two genotypes at the same treatment conditions (see Methods for detail). C, SuperVenn
1027 diagram of overlapped and specific DEGs at resting state (top), and PTI event (bottom). Note that normal ADF4
1028 complements *a234*, ADF-NLS majorly complements *a234* with a few extra DEGs, but ADF4-NES cannot complement
1029 *a234*. D, GO pathway enrichment analysis on genes DEGs among different groups. Selected pathways related to growth
1030 and metabolism, cell wall regulation, hormone, cytoskeleton, stresses (including immunity), and DNA processes are
1031 presented. ADF4 and ADF4-NLS contribute to DEGs in the pathways while ADF4-NES does not. DEGs in mock and flg22
1032 treated samples exhibit different patterns, suggesting partially distinguished role of nuclear ADF4 in different phases.
1033 E, SuperVenn diagram comparing ADF4-NLS regulated genes and ChIP-determined ADF4-targeted genes on promoters.
1034 A sum of 342 genes are both regulated and physically targeted by ADF4, as underlined. F, Distribution of ADF4-
1035 regulated TFs by protein family. ADF4-regulated genes are defined by the union set of DEGs between Col-0, *a234*/A4,
1036 and *a234*/A4-NLS vs *a234* in any condition. G, Summary of ADF-mediated transcriptional regulation.
1037
1038

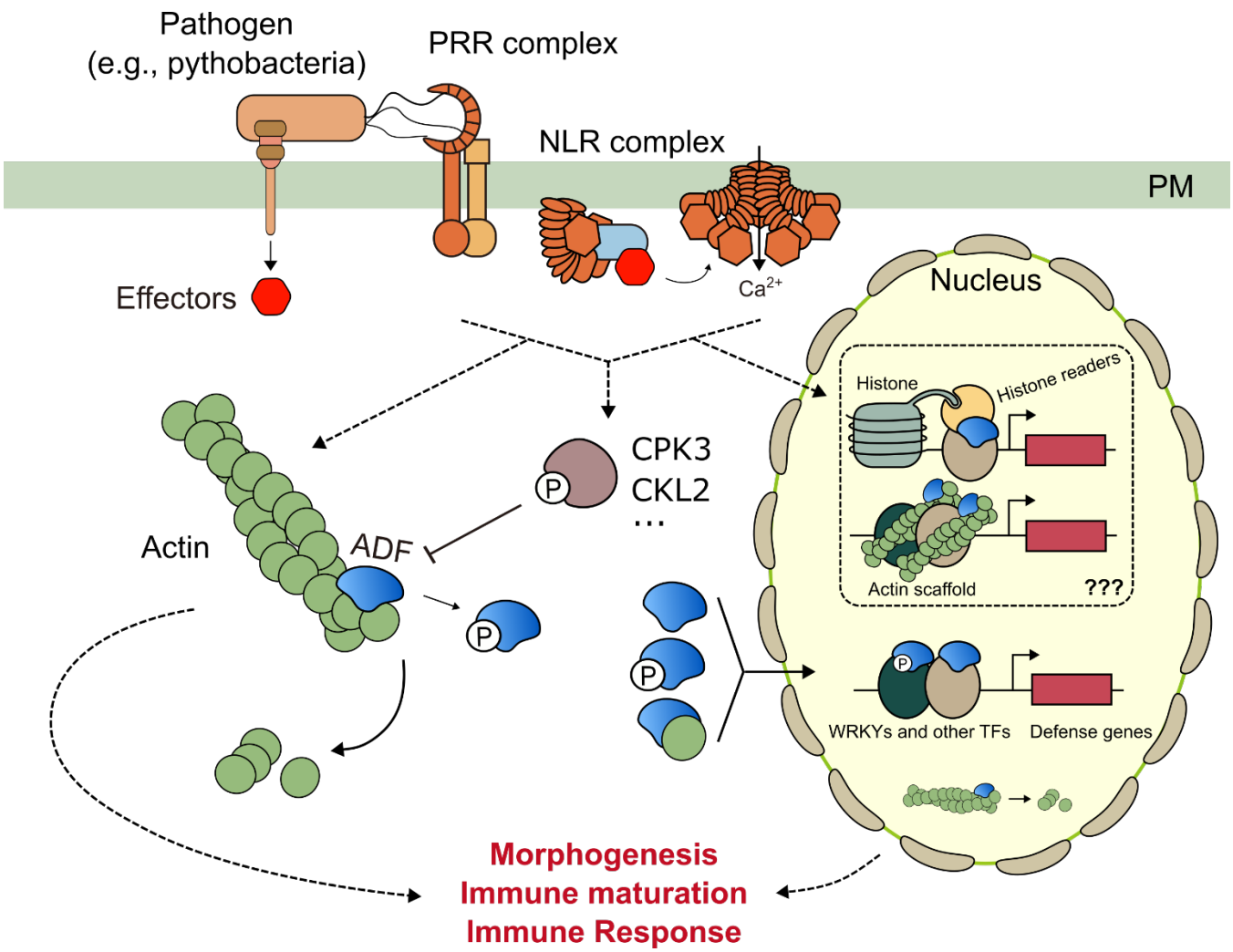

Figure 8: Proposed functional model describing the nuclear-cytosolic regulation of plant immunity by ADF. ADFs are duel-functional proteins by both (1) proceeding actin depolymerization, severing, or bundling in cytosol and (2) regulate transcriptional machinery in nucleus, as a moonlighting activity. These two activities utilize different protein-protein interaction interfaces on ADFs. Upon immune activation, ADF is phosphorylated by kinases such as CPK3 and CKL2, which blocks the ADF-actin interface and prohibit its actin depolymerization and changes actin dynamics, thereby remodeling the actin cytoskeleton to a pro-immune phase. On the other hand, ADFs interact with the transcriptional machinery in the nucleus, including transcription factors (such as WRKYs), histone and its associated proteins, and nuclear actin scaffold, which regulates the defense genes and multiple aspects within and beyond immunity. Phosphorylation on ADF upon immune activation may enhance the ADF nuclear function by either directly enhancing its binding affinity toward WRKYs or indirectly providing more nuclear ADFs dissociated from cytosolic ACT to drive the equilibrium to ADF-WRKY side. The combination of cytosolic and nuclear function of ADF synergistically shapes plant immunity (including immune maturation and immune response) and other aspects of plant development.